Derivation of diurnal courses of albedo and reflected solar irradiance from airborne POLDER data acquired near solar noon

Frédéric Jacob, Albert Olioso

XXXX

Derivation of diurnal courses of albedo and reflected solar irradiance from airborne PolDER data acquired near solar noon

Frédéric Jacob

(1) École Supérieure d'Agriculture de Purpan,

Laboratoire de Télédétection et de Gestion des Territoires,

Toulouse, France

(2) United States Department of Agriculture, Agricultural Research Service,

Hydrology and Remote Sensing Laboratory,

Beltsville, MD, USA

Albert Olioso

Institut National de la Recherche Agronomique,

Unité Climat - Sol - Environnement,

Avignon, France

Frédéric Jacob, École Supérieure d'Agriculture de Purpan, Laboratoire de Télédétection et de Gestion des Territoires, 75 voie du TOEC, 31076 TOULOUSE Cedex 3, France (frederic.jacob@esa-purpan.fr)

Albert Olioso, Unité Climat - Sol - Environnement, Institut National de la Recherche Agronomique, Domaine St Paul, Site Agroparc, 84914 Avignon Cedex 9, France (olioso@avignon.inra.fr)

Abstract. Knowledge of the diurnal course of land surface albedo is needed for monitoring radiative transfers between soil, vegetation and atmosphere. These transfers are of interest for crop monitoring, hydrological cycle modeling, weather forecast and climate modeling. The required absolute accuracy ranges between 0.02 and 0.05. At the present time, it is possible to derive the diurnal course of albedo from geostationary satellites. Sun - synchronous sensors, with higher spatial resolutions, allow retrieving surface radiative properties by both discriminating different types of land cover and capturing the subclass variability. However, the current possibilities for deriving the diurnal course of albedo from sun synchronous observations are empirical or mathematically complex. We proposed in this paper a physically based method, which is candidate for operational use along with multiangular sun - synchronous sensors, under clear sky conditions. This method uses both reciprocal Kernel - Driven Bi - directional Reflectance Distribution Function (KD BRDF) models and Narrowband To Broadband (NTB) conversion. It was implemented and validated using the Alpilles / ReSeDA database which was collected over agricultural areas. The implementation was performed using the 20 m spatial resolution airborne PolDER data acquired near midday. The validation was conducted using field measurements of albedo, recorded over the diurnal cycle. The retrievals of the diurnal course of albedo were good, with errors ranging from 0.026 to 0.029. Better results were observed for instantaneous values at solar noon and times close to satellite overpasses, as well as for the daily mean value, with errors ranging between 0.014 and 0.022. Amongst the selected reciprocal KD BRDF models, Li - Ross systematically provided the best results, regardless of considered albedo product. Further, using instantaneous values at times close to satellite overpasses, in place of the daily mean value, did not yield significant differences, with errors ranging around 0.01. Finally, we assessed the interest of deriving the diurnal course of reflected solar irradiance by using the several albedo products aforementioned. For the environmental conditions of the Alpilles / ReSeDA experiment, the resulting differences were not significant, with accuracies better than 20 $W.m^{-2}$.

1. Introduction

Land surface albedo is defined as the fraction of solar irradiance reflected within the upper hemisphere and over the whole solar spectrum [*Dickinson*, 1983; *Pinty and Verstraete*, 1992]. Since it directly drives the amount of solar irradiance absorbed by natural surfaces, its knowledge is of prime interest when studying surface net radiation budget and further energy transfers at the soil - vegetation - atmosphere interface. These transfers are of interest for crop monitoring [*Bastiaanssen and Chandrapala*, 2003], hydrological cycle modeling [*Ottlé and Vidal-Madjar*, 1994], weather forecast and climate modeling [*Noilhan and Lacarrere*, 1995; *Courault et al.*, 2003]. Retrieval of instantaneous albedo can be used to compute instantaneous surface energy fluxes [*Kustas and Humes*, 1997; *Kustas and Norman*, 1999; *Jacob et al.*, 2002a]. However, albedo is not constant during the day, mainly because of changes in solar position [*Dickinson*, 1983; *Dickinson et al.*, 1990; *Barnsley et al.*, 2000; *Grant et al.*, 2000]. This albedo variation has to be inferred for monitoring surface energy fluxes and evapotranspiration throughout the day [*Soer*, 1977; *Dickinson*, 1983; *Henderson-Sellers and Wilson*, 1983; *Jackson*, 1985; *Moran et al.*, 1994]. It is also required for the derivation of the daily mean value of albedo [*Grant et al.*, 2000]. Daily mean value of albedo is needed for monitoring daily evapotranspiration using the simplified relationship [*Seguin and Itier*, 1983; *Brasa-Ramos et al.*, 1998], as well as for the computation of the monthly value of albedo. Accurate values of albedo at daily or monthly scales are of interest for General Circulation Models (GCM) devoted to climate studies [*Dickinson et al.*, 1990; *Sellers et al.*, 1995; *Myhre and Myhre*, 2003; *Tian et al.*, 2004].

When dealing with accuracy requirements for GCM studies and weather forecast modeling, *Henderson-Sellers and Wilson* [1983] and *Cihlar et al.* [1997] proposed that an absolute accuracy of ± 0.05 is required. On the other hand, *Sellers et al.* [1995] suggested an absolute accu-

racy of ± 0.02, which corresponds to an accuracy on monthly averaged reflected solar irradiance of ± 10 W.m^{-2}. Estimating albedo at the hourly scale is of prime interest for the computation of the daily mean value of albedo. Indeed, *Grant et al.* [2000] showed that not considering the diurnal course of albedo yields an absolute error on the daily mean value up to 0.03, corresponding to 15% in relative terms. Similarly, *Kimes et al.* [1987] reported a 18% relative error on the daily mean value of reflected solar irradiance.

Visible - Near Infra Red (Vis - NIR) remote sensing is an attractive tool for estimating albedo under clear sky conditions. Indeed, it can provide maps at different spatial and temporal scales, whereas field measurements are not representative of the spatial variability depicted by land surfaces. Over the last two decades, several studies focused on estimating accurately land surface albedo from remotely sensed data. The proposed models have different degrees of complexity, leading to different types of approach: empirical, parametric, radiative or geometric (see the review by *Pinty and Verstraete* [1992]). Most of these approaches were devoted to the estimation of instantaneous albedo [*Brest and Goward*, 1987; *Dedieu et al.*, 1987; *Wanner et al.*, 1997; *Weiss et al.*, 1999; *Song and Gao*, 1999; *Lucht et al.*, 2000; *Liang*, 2000; *Zhao et al.*, 2000; *Pinty et al.*, 2000a; *Jacob et al.*, 2002b, c]. When the diurnal course is required, there are two possible approaches according to the use of geostationary or sun - synchronous sensors. For geostationary satellites which monitor a given location over the diurnal cycle, it simply consists of estimating instantaneous albedo within each interval of the temporal sampling [*Dedieu et al.*, 1987; *Pinty and Tanré*, 1987; *Minnis et al.*, 1997; *Pinty et al.*, 2000a, b]. Sun synchronous sensors, with higher spatial resolution, allow retrieving surface radiative properties by both discriminating different types of land cover and capturing the subclass variability. This is of interest for agricultural applications [*Baret et al.*, 2002]. Since these sensors collect, over

a given location, one observation a day when the platform overpasses, it is necessary to perform a temporal extrapolation. This can be done by empirically modeling the dependence of instantaneous albedo upon the sun position [*Barnsley et al.*, 2000; *Grant et al.*, 2000; *Lucht et al.*, 2000]. However, *Grant et al.* [2000] showed that this requires previous calibrations, whereas the solar dependence may vary significantly according to the observed target. Another possibility for the temporal extrapolation consists of using radiative transfer models [*Dickinson et al.*, 1990; *Liang and Strahler*, 1993; *Kimes et al.*, 2000]. However, inverting such models is mathematically complex and requires tedious numerical procedures, which is not appropriate for operational applications [*Wanner et al.*, 1997; *Pragnère et al.*, 1999; *Kimes et al.*, 2000].

Regarding limitations of the current possibilities for sun - synchronous sensors, reciprocal Kernel - Driven Bi - directional Reflectance Distribution Function (KD BRDF) models offer the opportunity to investigate new approaches devoted to the retrieval of the diurnal course of albedo. These models are physically based and designed for operational use. Both their basic concepts and features are reviewed in *Lucht and Roujean* [2000], and will be summarized in this paper (§ 4.1 and § 4.2). Promising results were already reported when using reciprocal KD BRDF models, along with single directional data collected from geostationary sensors at different solar positions during the day [*van Leeuwen and Roujean*, 2002; *Pokrovsky et al.*, 2003a, b]. For multidirectional sun - synchronous sensors, these models have been used to retrieve instantaneous albedo products from multiangular data collected at a given solar position of the day [*Lucht*, 1998; *Weiss et al.*, 1999; *Schaaf et al.*, 2002; *Jacob et al.*, 2002b, c].

This study focused on implementing and validating a new approach devoted to the derivation of the diurnal course of albedo from multidirectional data collected at a given time of the day. The method we propose is candidate for operational use along with multiangular sun -

synchronous sensors, under clear - sky conditions. It is a physically based procedure that relies on the use of both reciprocal KD BRDF models and Narrowband To Broadband (NTB) conversion. NTB conversion consists of expressing integrated values of broadband albedo as linear combinations of narrowband multispectral observations provided by remote sensors. Detailed description and analysis of NTB conversion are given in *Brest and Goward* [1987]; *Liang et al.* [1999, 2002b]; *Jacob et al.* [2002b, c], and will be summarized in this paper (see § 4.5). The method we propose was tested over the data set gathered in the framework of the Remote Sensing Data Assimilation (ReSeDA) program [*Prévot et al.*, 1998; *Olioso et al.*, 1998; *Baret*, 2000]. The Alpilles - ReSeDA experiment combined acquisition during one year of 1/ multiangular Vis - NIR remote sensing data collected near midday twice a month with the airborne POLDER sensor, and 2/ ground based measurements of albedo recorded throughout the day within several agricultural fields (§ 3). The use of high spatial resolution and multitemporal remotely sensed data allowed us to validate albedo retrievals over cycles of several crops.

The current paper is structured as following. In a first part, we detail:

- the definitions to be used in the paper (§ 2),
- the Alpilles / ReSeDA project, its goals and experimental support (§ 3.1),
- the acquisition and preprocessing of the ReSeDA / PolDER dataset (§ 3.2),
- the ground based measurements of albedo used for validation exercises (§ 3.3).

Implementing the method we propose over the ReSeDA data set was performed as following.

- According to performance studies reported in the literature, we selected reciprocal Kernel - Driven (KD) BRDF models (§ 4.1 and 4.2).
- The models were inverted over the PolDER BRDF angular samplings near midday (§ 4.3).

• The inverted models were forwardly run to compute, within each PolDER channel, hemispherical reflectance (also called spectral or narrowband albedo) for different solar positions over the diurnal cycle (§ 4.4).

• The diurnal course of broadband albedo was derived from those of hemispherical reflectance by using Narrowband To Broadband (NTB) conversion (§ 4.5).

Section 5 presents the strategy used to analyze and validate the method we propose over the Alpilles - ReSeDA data set. The results are presented as following.

• The analysis of field data of albedo are reported in § 6.1.

• We assessed the robustness of the reciprocal KD BRDF models regarding the temporal extrapolation, by considering hemispherical reflectance (§ 6.2) and albedo (§ 6.3).

• We next focused on reflected solar irradiance which is the albedo - linked component of land surface radiation budget (§ 6.4).

Retrievals of albedo and reflected solar irradiance were validated by considering specific albedo products: the diurnal course, the daily mean value, and typical instantaneous values (10:00, 12:00 and 14:00 local solar time). Finally, the results are discussed regarding observations reported in previous studies (§ 7).

2. Definitions and nomenclature

Over the last decade, several studies focused on albedo retrieval from remote sensing, which yielded the existence of different nomenclatures. In this section, we first define the variables of interest: surface radiative properties and remote sensing measurements. These definitions are given by linking them to nomenclatures proposed in the literature.

The definition of albedo $a(\theta_s, \varphi_s)$ as the fraction of solar irradiance reflected within the upper hemisphere and over the whole solar spectrum may be expressed as [*Weiss et al.*, 1999]:

$$a(\theta_s, \varphi_s) = \frac{\int_{300\ nm}^{3000\ nm} \rho_{h,\lambda}(\theta_s, \varphi_s)\ R_{g,\lambda}(\theta_s, \varphi_s)\ d\lambda}{\int_{300\ nm}^{3000\ nm} R_{g,\lambda}(\theta_s, \varphi_s)\ d\lambda} \quad (1)$$

This definition accounts for the reflected fractions of diffuse and direct solar irradiances, and can be labeled shortwave apparent albedo [*Liang et al.*, 1999; *Liang*, 2000; *Liang et al.*, 2002b]. Hemispherical reflectance $\rho_{h,\lambda}(\theta_s, \varphi_s)$ represents the fraction of spectral solar irradiance $R_{g,\lambda}(\theta_s, \varphi_s)$ reflected within the upper hemisphere, for a given wavelength λ, and a given solar direction characterized by zenith and azimuth angles (θ_s, φ_s). Spectral solar irradiance $R_{g,\lambda}(\theta_s, \varphi_s)$, also called incoming solar radiation, includes diffuse and direct components. Consequently, hemispherical reflectance $\rho_{h,\lambda}(\theta_s, \varphi_s)$ includes reflected fractions of solar direct and diffuse irradiances: it corresponds to the weighted sum of directional - hemispherical and hemispherical - hemispherical (bi - hemispherical) reflectances, the weighting coefficients being the fractions of direct and diffuse solar irradiances [*Lucht et al.*, 2000]. Directional - hemispherical and hemispherical - hemispherical reflectances are also called black - sky and white - sky albedos [*Lucht*, 1998; *Wanner et al.*, 1997; *Lucht et al.*, 2000; *Schaaf et al.*, 2002; *Pokrovsky et al.*, 2003a]. Hemispherical reflectance $\rho_{h,\lambda}(\theta_s, \varphi_s)$ is also labeled spectral albedo, or spectral apparent albedo [*Kimes and Sellers*, 1985; *Kimes et al.*, 1987; *Privette et al.*, 1997; *Toll et al.*, 1997; *Weiss et al.*, 1999; *Liang et al.*, 1999; *Lucht and Roujean*, 2000; *Liang et al.*, 2002b].

Hemispherical reflectance $\rho_{h,\lambda}(\theta_s, \varphi_s)$ can be expressed as the integration over viewing zenith and azimuth angles (θ_v, φ_v) of apparent bi - directional reflectance $\rho_\lambda(\theta_s, \varphi_s, \theta_v, \varphi_v)$:

$$\rho_{h,\lambda}(\theta_s, \varphi_s) = \frac{1}{\pi} \int_0^{2\pi} \int_0^{\pi/2} \rho_\lambda(\theta_s, \varphi_s, \theta_v, \varphi_v)\ \cos(\theta_v)\ \sin(\theta_v)\ d\theta_v\ d\varphi_v \quad (2)$$

where apparent bi - directional reflectance $\rho_\lambda(\theta_s, \varphi_s, \theta_v, \varphi_v)$ is the weighted sum of directional - directional (bi - directional) and hemispherical - directional reflectances, the weighting coefficients being the fractions of direct and diffuse solar irradiances. Then, the angular distribution of bi - directional reflectance (respectively apparent bi - directional reflectance) corresponds to BRDF for Bi - directional Reflectance Distribution Function (respectively apparent BRDF).

Remote sensors provide, after atmospheric corrections, data of apparent bi - directional reflectance within given wavebands characterized by filter response functions. The albedo retrievals within these wavebands are often called narrowband albedos, whereas integrated values over given portions of the solar spectrum are usually labeled broadband albedos [*Russel et al.*, 1997; *Song and Gao*, 1999; *Lucht et al.*, 2000; *Barnsley et al.*, 2000; *Liang et al.*, 2002a, b].

In the current study, we use the following labels: albedo for shortwave apparent albedo, hemispherical reflectance for narrowband apparent albedo, bi - directional reflectance for the remote sensing measurements of apparent bi - directional reflectance, and BRDF for the angular distribution of apparent bi - directional reflectance (apparent BRDF).

3. Data acquisition and preprocessing

3.1. The experiment

The data were collected during the Alpilles - ReSeDA experiment, which was the first step of the European ReSeDA program. This program aimed at improving the use of multitemporal, multispectral and multidirectional remote sensing data for a better understanding and description of soil and vegetation processes [*Prévot et al.*, 1998; *Baret*, 2000]. It focused on assimilating remotely sensed data into both Soil - Vegetation - Atmosphere - Transfer (SVAT) and crop simulation models. Moreover, the simultaneous acquisition of remote sensing data at

different spatial resolutions allowed assessing the scaling issue, i.e. the meaning of aggregated variables when using coarse resolution sensors [*Olioso et al.*, 1998; *Wassenaar et al.*, 2002].

The study area was a Mediterranean agricultural region of 5×5 km^2 size, located in the South East of France (N 43°47', E 4°45'). Field sizes were 200×200 m^2. Main crops were maize, sunflower, wheat and alfalfa. During the experiment that lasted from November 1996 to November 1997, several airborne and spaceborne remote sensing data were acquired over solar, thermal infrared and microwave domains. Simultaneously, numerous field data characterizing the soil - vegetation - atmosphere interface were collected daily at seven locations within crops of winter wheat (Fields 101 and 120), spring wheat (Field 214), sunflower (Fields 102, 121 and 501), and alfalfa (Field 203). A detailed description of the experimental setup is given by *Olioso et al.* [2002]. In the current study, we focused on 1/ the visible - near infrared remote sensing data acquired with the airborne PolDER sensor, and 2/ the field measurements of albedo.

3.2. PolDER data

The airborne PolDER imaging radiometer flew once to twice a month. Data were collected on clear sky days at a 3000 m flight altitude which yielded a 20 m nadir spatial resolution. For each day of acquisition, four flight lines were parallel to the solar plan, and one was perpendicular. The five flight lines were completed within 45 minutes centered around solar noon: the central hour of PolDER data acquisition was usually close to local solar noon, but ranged between 11:15 and 14:00 local solar time, according to the day of experiment. PolDER provided measurements of bi - directional reflectance over four wavebands centered at 443, 550, 670 and 865 nm (40 nm width). View zenith angle ranged from 0 to 45°, with a 0.4° resolution. Each measurement was collected with informations from a Global Positioning System (GPS) and a Gyroscopic Central Unit (GCU), for the computation solar position and viewing direction.

The PolDER data were preprocessed in a similar way to that used by *Leroy and Hautecoeur* [1999]. A detailed description can be found at `http://www.avignon.inra.fr/reseda/base/documents/reseda-report/RES-111.pdf`. The sensor calibration was performed before, during and after the experiment. Its accuracy was about 5%. Atmospheric effects were removed using the Simplified Method for Atmospheric Correction (SMAC) algorithm [*Rahman and Dedieu*, 1994]. SMAC computed bi - directional reflectance by ratioing reflected solar radiance in the viewing direction to incoming solar irradiance, the latter including the diffuse and direct components. Using the data collected from the GPS and the GCU, images were superimposed to a Lambert II projection, which corresponded to a 20 m spatial sampling. All these preprocessing provided, for each day of the experiment, each of the 20 m size pixels within the 5×5 km^2 size study area, and each of the four PolDER channels, an angular sampling of BRDF between 0 and 45°, each sample corresponding to a solar position.

3.3. Field data of albedo

The *in - situ* albedo data were calculated as the ratio of reflected to incoming solar radiation measurements. Solar irradiance was measured using a Kipp & Zonen CM6B pyranometer, setup on a meteorological site located on the center of the study area. Two other measurements on different locations provided very close measurements: correlation coefficient of 0.999, and mean quadratic error of 10 W.m^{-2}, corresponding to 1% in relative terms.

Data of reflected solar irradiance were available for six of the seven ground measurement stations (Fields 101, 102, 120, 203, 214, 501). These data were collected near field centers, with a 15 s time step and a 20 mn averaging. Their ground footprint ranged from 1000 to 3000 m^2, depending on sensor height. Two kinds of devices were used to measure reflected solar irradiance: Kipp & Zonen CM6B and Skye SP1110 sensors. The features of the SKYE sensors

required a spectral extrapolation, which was set as a linear relation between simulated Kipp & Zonen CM6B and Skye SP1110 albedo products. Both albedo simulations and relationship calibration are described in details by *François et al.* [2002] and *Jacob et al.* [2002b, c].

4. Deriving the instantaneous value, the diurnal course and the daily mean value of albedo

In this section, we present the implementation of the proposed method over the Alpilles - ReSeDA / PolDER multidirectional dataset. We first give a brief overview of the Kernel - Driven Bi - directional Reflectance Distribution Function (KD BRDF) models, to next select some of them according to the study objectives. Then, we explain the computation of hemispherical reflectance products: instantaneous value and diurnal course. Finally, we present the derivation of PolDER albedo products: instantaneous value, diurnal course and daily mean value.

4.1. Kernel - Driven BRDF models: a brief presentation

KD BRDF models aim at deriving the whole BRDF from angular samplings provided by multiangular remote sensing data. These models express the observed BRDF as a superposition of BRDF basic shapes. Each shape correspond to a radiative transfer process: isotropic reflection, surface reflection and volume scattering [*Roujean et al.*, 1992; *Wanner et al.*, 1995, 1997; *Lucht and Roujean*, 2000; *Lucht et al.*, 2000]. The BRDF basic shapes are expressed using mathematical functions (kernels). The bi - directional reflectance is then given as a linear combination of the N kernels K_i which depend on the viewing angles (θ_v, φ_v), and the solar angles (θ_s, φ_s):

$$\rho_\lambda(\theta_s, \varphi_s, \theta_v, \varphi_v) = \sum_{i=1}^{N} \alpha_{i,\lambda}\, K_i(\theta_s, \varphi_s, \theta_v, \varphi_v) \tag{3}$$

The coefficients $\alpha_{i,\lambda}$ depend on wavelength λ and the radiative properties of the observed surface. From a multiangular dataset of bi - directional reflectance ρ_{λ_j} collected over a given location for a given solar position, and within a given waveband j, inverting a KD BRDF model

consists of estimating rapidly and unambiguously the coefficients α_{i,λ_j} by solving the system $[\rho_{\lambda_j}] = [K][\alpha_{i,\lambda_j}]$ through a pseudo - matrix inversion. Once inverted, the model can be forwardly run for a given solar position and for several viewing angles within the upper hemisphere, which provides the BRDF retrieval. Both model inversion and forward run are fast and easy to implement, which makes KD BRDF models candidates for operational use.

KD BRDF models can be split in two categories according to their reciprocity properties, i.e. the possibility or not to switch solar and viewing angles. This yields labeling KD BRDF models as "reciprocal" or "non reciprocal". The consequence of reciprocity properties is the independence of inversion coefficients to solar position.

• Non reciprocal KD BRDF models, such as the Walthall model [*Walthall et al.*, 1985], have kernels which do not fully account for the solar position. The inversion procedure provides coefficients which depend on the solar direction. Retrieving the diurnal course of BRDF requires inverting the model over datasets collected at different solar positions over the diurnal cycle.

• Reciprocal KD BRDF models, such as Roujean [*Roujean et al.*, 1992] and Li - Ross [*Wanner et al.*, 1995], have kernels which fully account for the solar position. The inversion procedure provides coefficients which do not depend on the solar direction. It is possible to compute BRDF at any solar position, regardless of solar position for model inversion.

4.2. Rationale in choosing Kernel - Driven BRDF models

In the current study, the diurnal course of albedo was derived from that of hemispherical reflectance which was inferred from that of BRDF. Therefore, we had to consider reciprocal KD BRDF models only. Choosing models was driven by results reported in previous studies, which dealt with the model performances when 1/ retrieving the observed BRDF, and 2/ deriving hemispherical reflectance. We considered three classical models: Li - Ross [*Wanner et al.*,

1995], Modified Rahman Pinty Verstraete (MRPV) [*Engelsen et al.*, 1996], and Roujean [*Roujean et al.*, 1992]. These models have three kernels, hence three coefficients $\alpha_{i,\lambda}$ in Equation 3.

Four variants were proposed for Li - Ross, according to the canopy density and thickness. We considered the "Li - Sparse / Ross - Thick" version, which was selected by *Wanner et al.* [1997] for its performances over plowed fields and vegetated surfaces, and presented as one of the most accurate models by *Privette et al.* [1997] and *Lucht* [1998]. Amongst the two available versions for MRPV, we choose the linearized version which inversion procedure is easier and faster [*Engelsen et al.*, 1996], while this variant provided good results from validation exercises [*Baret et al.*, 1997; *Lucht*, 1998; *Weiss et al.*, 2002b]. Roujean was previously tested over several measured and simulated data sets, and presented as a robust model [*Baret et al.*, 1997; *Chopping*, 2000; *Pokrovsky and Roujean*, 2002; *Pokrovsky et al.*, 2003a]. We did not consider the reciprocal version of the Walthall model proposed by *Nilson and Kuusk* [1989], since *Lucht* [1998] showed this version provided poor retrievals for BRDF and hemispherical reflectance.

The three reciprocal KD BRDF models we selected were already tested over the Alpilles - ReSeDA / PolDER data set for the derivation of instantaneous products at the PolDER data acquisition time. First, *Weiss et al.* [2002b] showed expressing the observed BRDF from three kernels was sufficient, since they contain up to 95% of the required information. They reported the model fitting performances were better if the inversion was performed over samplings within the solar plan. Second, *Jacob et al.* [2002b] showed the model performances were not driven by atmospheric conditions. They observed the retrieval quality for the hemispherical reflectance was driven by the model performances for viewing extrapolation outside the PolDER angular sampling. Third, *Jacob et al.* [2002b, c] showed that these reciprocal KD BRDF models provide

close retrievals of hemispherical reflectance at the PolDER data acquisition time, with relative discrepancies ranging between 8 and 12% according to the PolDER channel.

4.3. Inverting reciprocal KD BRDF models over PolDER data

The selected models were inverted over the multidirectional ReSeDA / PolDER dataset. The latter provided, for each day of the experiment, each of the 20 m size pixels, and each of the four PolDER channels, an angular sampling of BRDF between 0 and 45°. Model inversion was performed on a pixel by pixel basis, over these multidirectional measurements of bi - directional reflectance $\rho_\lambda(\theta_s, \varphi_s, \theta_v, \varphi_v)$. The models fully accounted for the solar position (§ 4.1). Therefore, their inversion was performed considering the solar position for each of the measurements collected within the PolDER data acquisition period (45 minutes, see § 3.2).

In this paper we used the label bidirectional reflectance for PolDER measurements of apparent bidirectional reflectance (§ 2). Following standard procedures reported in the literature [*Roujean et al.*, 1997; *Wanner et al.*, 1997; *Privette et al.*, 1997; *Lucht*, 1998; *Chopping*, 2000; *Weiss et al.*, 2002b], we inverted the reciprocal KD BRDF models over the angular samplings of apparent BRDF. The latter included directional - directional and hemispherical - directional reflectances, each weighted by the direct and diffuse solar irradiances at the PolDER data acquisition time (§ 2). From our understanding of the considered processes, integrating the retrieved apparent BRDF provided apparent albedo, although it corresponded to black-sky albedo, according to literature. This yield assuming, when deriving the diurnal course of albedo, a constant diurnal course for the ratio of diffuse to direct solar irradiances, equal to that for PolDER data acquisition. This assumption relied on close values for black sky and apparent albedo, as discussed further: the environmental conditions corresponded to low diffuse solar irradiance (§ 6.1), whereas the latter did not significantly influence albedo computation (§ 7).

4.4. Deriving the diurnal course of hemispherical reflectance

The inverted models were next forwardly run, to retrieve bi - directional reflectance at any solar and viewing directions. BRDF was then computed for different solar positions between sunset and sunrise, with a 20 mn time step corresponding to that of field data acquisition (§ 3.3). Solar zenith and azimuth angles were calculated from astronomical rules using the latitude - longitude of the site and the local solar time. The calculations were actually limited to solar zenith angles ranging from 0 to 80°, because of unrealistic retrievals for larger solar zenith angles. This was ascribed to the model physics which become questionable for such angles [*Lucht*, 1998]. The 80° limitation on sun zenith angle could be applied since solar irradiance was low for these angles: according to field measurements, solar irradiance integrated over sun zenith angles larger than 80° was about 5% of that integrated over the diurnal cycle.

Hemispherical reflectance within each PolDER channel $\rho_{h,\lambda_j}(\theta_s, \varphi_s)$ was derived by integrating the retrieved BRDF over viewing angles (θ_v,φ_v) (see Equation 2). According to the model used, the integration was analytical, or numerical over a 24×24 direction Gaussian quadrature [*Weiss et al.*, 1999]. These calculations provided, for each day of the experiment, each of the 20 m size pixels, and each of the four PolDER channels, the diurnal course of hemispherical reflectance, with a 20 mn time step, and for solar zenith angles ranging between 0 and 80°.

For assessing the method proposed in this paper, we also considered the retrieval of instantaneous hemispherical reflectance at the PolDER data acquisition time. We forwardly run the inverted models, to compute instantaneous BRDF over the data collection period which lasted 45 minutes around solar noon (§ 3.2). This required averaging, over this period, the solar position to be used for the calculation of BRDF [*Jacob et al.*, 2002b, c].

4.5. Computing PolDER albedo products

Integrated values of broadband albedo can be expressed as linear combinations of narrowband multispectral observations using Narrowband To Broadband (NTB) conversion (see Introduction). Therefore, the diurnal course of albedo was derived applying NTB conversion to those of hemispherical reflectance within the four PolDER channels. The integrated value of albedo over the whole solar spectrum was expressed as a linear combination of hemispherical reflectance $\rho_{h,\lambda_j}(\theta_s, \varphi_s)$ within the four PolDER channels j centered at 443, 550, 670 and 865 nm:

$$a(\theta_s, \varphi_s) = \sum_{j=1}^{j=4} \beta_{\lambda_j} \rho_{h,\lambda_j}(\theta_s, \varphi_s) \quad (4)$$

No coefficient set β_{λ_j} was proposed for the airborne PolDER sensor. When estimating instantaneous albedo at the PolDER data acquisition time, *Jacob et al.* [2002b, c] considered several sets proposed in the literature for others sensors having spectral configurations similar to that of PolDER. They showed, through a detailed analysis of validation results, that the most adequate coefficient set was that proposed by *Liang et al.* [1999] for MISR atmospherically corrected data (see Table 1). This coefficient set allowed retrieving instantaneous albedo at the PolDER data acquisition time with an Absolute Root Mean Square Error (ARMSE[6]) of 0.0188, corresponding to a Relative Root Mean Square Error (RRMSE[7]) of 9.5%. The obtained accuracy fulfilled requirements for further applications, since it was lower than 0.02 in absolute (see Introduction). Therefore, we considered this set when deriving 1/ instantaneous albedo at the PolDER data acquisition time, and 2/ the diurnal course of albedo.

Table 1

From the retrieved diurnal course of albedo, we finally derived the daily mean value of albedo $< a >$ by weighting each instantaneous estimate $a(\theta_s, \varphi_s)$ with the corresponding solar irradiance $Rg(\theta_s, \varphi_s)$:

[6] ARMSE is the mean quadratic difference between predictions and observations for a given variable.
[7] RRMSE is the ratio of ARMSE to the mean value of the observations.

$$< a >= \frac{\int_{t=t_r}^{t=t_s} Rg(t)\, a(t)\, dt}{\int_{t=t_r}^{t=t_s} Rg(t)\, dt} \simeq \frac{\sum_{i=1}^{i=M} Rg(\theta_{si}, \varphi_{si})\, a(\theta_{si}, \varphi_{si})}{\sum_{i=1}^{i=M} Rg(\theta_{si}, \varphi_{si})} \quad (5)$$

where dt is the time step equal to 20 minutes (§ 4.4), $(\theta_{s1}, \varphi_{s1})$ are solar zenith and azimuth angles (θ_s, φ_s) at sunrise time $t = t_r$, and $(\theta_{sM}, \varphi_{sM})$ are (θ_s, φ_s) at sunset time $t = t_s$.

5. Strategy for analyzing and validating the proposed method

In the context of deriving the diurnal course of albedo from multiangular data set collected at a given time of the day, we assessed the abilities of the reciprocal KD BRDF models to perform a temporal extrapolation. Since the diurnal course of albedo was derived from that of hemispherical reflectance (§ 4.5), we analyzed the retrievals of first hemispherical reflectance (§ 6.2), and second albedo (§ 6.3). Finally, we focused on the diurnal course of reflected solar irradiance (§ 6.4), which is the albedo linked component for land surface radiation budget.

When focusing on albedo and reflected solar irradiance, we assessed the utility of considering either the diurnal course of albedo, the daily mean value, or instantaneous values at specific times (10:00, 12:00 and 14:00 local solar time). These times were close to satellite overpasses: SPOT, Landsat, Terra on morning, and Aqua, NOAA on afternoon. The resulting albedo products were first validated against ground based measurements. Next, they were used for the derivation of the diurnal course of reflected solar irradiance, the latter being then validated.

We also considered the albedo retrievals at the PolDER data acquisition time (§ 4.4). This aimed at linking the retrieval quality for the diurnal course of albedo to that for instantaneous values over the information collection period (45 minutes around solar noon, see § 3.2). For this, instantaneous albedo was retrieved by averaging over this period 1/ field measurements of albedo recorded with a 20 minute step (§ 3.3), and 2/ the solar position to be used for the calculation of the hemispherical reflectance (§ 4.4).

The investigations listed above were conducted considering the six PolDER pixels which matched the ground based measurement locations (§ 3.3). Therefore, we compared 20 m^2 size PolDER pixels against field measurements with footprints ranging from 1000 to 3000 m^2. This was possible since the spatial variability of the PolDER albedo products within the field measurement footprints was not significant [*Jacob et al.*, 2002b].

6. Results

6.1. Field data of albedo

First subplot of Figure 1 displays the diurnal courses of incoming and reflected solar radiation measured inside Field 203 (alfalfa crop). The considered days were those corresponding to PolDER data acquisition. The curves showed measurements were fluctuating on days 05/22, 06/09 and 06/24, the corresponding diurnal courses of albedo being perturbed (see second subplot). This was ascribed to atmospheric perturbations such as clouds overpassing the study area. Reciprocal Kernel - Driven (KD) BRDF models were not designed to account for such atmospheric perturbations occurring throughout the day. Therefore, the data collected during these three days were removed, which yielded selecting days with low diffuse solar irradiances.

Figure 1

Second subplot of Figure 1 displays asymmetries between morning and afternoon albedo profiles. Such asymmetries were observed with previous experiments by, for instance, *Minnis et al.* [1997] and *Song* [1998]. They gave as explanations several factors: change in crop architecture, vegetation alignment, minor changes in atmospheric conditions, morning dew, evaporation or wind. To quantify the observed asymmetries, we intercompared the instantaneous albedo values at symmetric times to solar noon, i.e. 10:00 and 14:00 local solar time. These values were very close (see Figure 2), as shown by statistical indicators:

Figure 2

- coefficient correlation of 0.92,

- Absolute and Relative Root Mean Square Difference (ARMSD[1] and RRMSD[2]) of 0.009 and 4.3% respectively,
- Absolute and Relative Bias (ABias[3] and RBias[4]) of 5e-4 and 0.2% respectively,
- offset / slope values of 0.03 and 0.88 respectively, if expressing the 14:00 value as a linear function of the 10:00 value.

Finally, we assessed the uncertainties induced by using, in place of the daily mean value of albedo, the instantaneous values at 12:00, 10:00 and 14:00 local solar time (Figure 3). The noon and daily mean values were different (right subplot), with ARMSE and ABias values of 0.021 and -0.019, respectively. The instantaneous values at 10:00 agreed very well with the daily mean value (bottom left subplot). Using the instantaneous values at 10:00 and 14:00 local solar time, rather than the daily mean value, induced low errors (left subplots): ARMSE = 0.007 / ABias = -0.006 and ARMSE = 0.010 / ABias = -0.007, respectively.

Figure 3

6.2. Hemispherical reflectance within the PolDER channels

We next assessed the consistencies of the reciprocal KD BRDF models for extrapolating, over the diurnal cycle, the remote sensing information collected at a given time of the day. For this, we analyzed the retrieved diurnal courses of hemispherical reflectance. Figure 4 displays examples of diurnal courses of hemispherical reflectance retrieved from Li - Ross and Roujean over a bare soil and a wheat crop. The bowl shape of the diurnal course of hemispherical reflectance at 865 nm was more pronounced for the wheat crop (right subplots), than for bare soil (left subplots). A converse behavior was observed for the other channels. For both surfaces,

Figure 4

[1] ARMSD is the mean quadratic difference between two different predictions for a given variable.
[2] RRMSD is the ratio of ARMSD to the mean value of the two predictions.
[3] ABias is the mean difference between two different predictions for a given variable.
[4] RBias is the ratio of ABias to the mean value of the two predictions.

hemispherical reflectance was larger at 865 nm than for the other PolDER channels. This trend was more pronounced for the wheat crop. The diurnal courses of hemispherical reflectance retrieved from Li - Ross and Roujean could be significantly different. For NIR hemispherical reflectance over bare soil, the absolute difference ranged from 0.04 at noon to 0.1 at sunrise and sunset, which corresponded to relative differences of 25% and 40%, respectively.

The four subplots on Figure 4 showed the differences between model retrievals depended on the surface type, the wavelength, and the solar direction. To characterize these differences as functions of the wavelength and the solar direction, we used the following protocol. For each day, each of the 6 validation pixels, and each PolDER channel, the discrepancies between model retrievals were characterized as a functions of the local solar time. By using three reciprocal KD BRDF models, there were three hemispherical reflectance retrievals to be compared for a given solar time i. The discrepancy was characterized using the Absolute Range (AR) and the Relative Range (RR) for the hemispherical reflectance retrievals ρ_{hi}: $AR_i = \max(\rho_{hi}) - \min(\rho_{hi})$, and $RR_i = \frac{AR_i}{\overline{\rho_{hi}}}$, where $\overline{\rho_{hi}}$ is the averaged value of the three model retrievals.

Figure 5 displays, for the alfalfa crop, variations of the Absolute Range (AR) and the Relative Range (RR) versus the local solar time. The main trend was an increase of the AR and RR values, as the solar zenith angle increased. A decrease of the AR and RR values for the same solar changes was sometimes observed at 550 and 670 nm, on summer days. For a better understanding of the trends we observed with the alfalfa crop, we next considered all fields for a given day and all days for a given field. The trends were similar, but we did not observed any systematical behavior. Overall, the averaged values of the Relative Range over the experiment were 70%, 20%, 23%, and 9%, for PolDER channels at 443, 550, 670, and 865 nm, respectively.

Figure 5

6.3. PolDER albedo products

The diurnal course of albedo were derived using the three reciprocal KD BRDF models along with the NTB conversion coefficient set designed for MISR observations (§ 4.5). This yielded three different retrievals for the diurnal course of albedo. Their intercomparison was performed using a similar protocol to that used for hemispherical reflectance. The discrepancy between the retrievals was analyzed through Absolute Range (AR) and Relative Range (RR) as functions of the local solar time (§ 6.2). The trends were similar to those observed for hemispherical reflectance. Nevertheless, we noted a significantly lower occurrence of decreasing AR and RR values as the solar zenith angle increased (figure not shown). The AR values ranged between 0.005 and 0.04, i.e. from 3 to 25% in relative terms. Overall, the RR averaged value over the experiment was 0.016, i.e. 10% in relative.

Examples of comparison of PolDER retrievals against field measurements for the diurnal course of albedo are displayed in Figure 6. Despite some differences between predictions and observations, the proposed method provided consistent estimates. The general trend was an increase of the difference between PolDER retrievals and field data, as the solar zenith angle increased. The diurnal courses retrieved with the Li - Ross model were systematically flatter than those derived from the other models. These scatterplots suggested the bias between PolDER retrievals and field measurements over the diurnal cycle might be driven by that occurring at the PolDER data acquisition time. This was verified through a 0.8 correlation coefficient.

Figure 6

Table 2 displays the validation results for PolDER products when considering the instantaneous value at the PolDER data acquisition time, the diurnal course, the instantaneous value at solar noon, and the daily mean value. PolDER retrievals of the instantaneous values at data acquisition time and solar noon were very good, as compared to the desired accuracy (0.02-0.05): ARMSE ranged between 0.0141 and 0.0201 according to the model, corresponding to 6.5 and

Table 2

9.3%, in relative terms. For the diurnal course, the validation results were less good. Absolute errors ranged between 0.0260 for Li - Ross and 0.0285 for Roujean, corresponding to relative errors of 12 and 13%. For the daily mean value, ARMSE range was [0.170 - 0.260], which was intermediate between that for the instantaneous value at solar noon and that for the diurnal course. Besides, the underestimation of the field data by PolDER / Li - Ross products was larger for the daily mean value than for the noon value. Regardless of considered albedo product, the best (respectively worst) retrievals systematically corresponded to the Li - Ross (resp Roujean) reciprocal KD BRDF model. We note the validation results reported here for instantaneous albedo were slightly different from those reported by *Jacob et al.* [2002b, c]. Indeed, by filtering data to select environmental conditions allowing the retrieval the diurnal course of albedo, we removed a part of the days and fields considered in these studies (§ 3.3 and 6.1).

Figure 7 displays the validation scatterplots for two PolDER / Li - Ross albedo products: the instantaneous value at solar noon and the daily mean value. The trends were very similar for both products: large correlations, low discrepancies, and underestimations of field data by PolDER retrievals. These two albedo products were finally intercompared (Figure 8). The results were very consistent with those obtained for field data (§ 6.1 and Figure 3). The noon and daily mean values were different, with ARMSE and ABias values of 0.015 and 0.013.

Figure 7

6.4. PolDER products of reflected solar irradiance

The method we propose here was finally validated considering the diurnal course of reflected solar irradiance. We assessed its accuracy by validating, against field measurements, retrievals derived from the following albedo products: 1/ the diurnal course, 2/ the daily mean value, 3/ instantaneous values at 10:00, 12:00 and 14:00 local solar time. Since validation results for

albedo retrievals were systematically better with Li - Ross (§ 6.3), the investigations dealing with reflected solar irradiance were conducted considering the Li - Ross albedo products only.

Figure 9 displays the validation results for the diurnal course of reflected solar irradiance derived by using the diurnal course, the noon and the daily mean values of albedo. The PolDER / Li - Ross retrievals closest to the field references were obtained with the diurnal course. The use of the instantaneous albedo at solar noon induced an underestimation of reflected solar irradiance over the diurnal cycle, mainly for intermediate solar zenith angles. The use of the daily mean value induced a large scatter around solar noon.

Figure 9

Table 3 displays ABias and ARMSE when comparing, against field measurements, reflected solar irradiance retrieved from PolDER by using the several Li - Ross albedo products previously listed. ARMSE ranged from 11.5 $W.m^{-2}$ to 17 $W.m^{-2}$, corresponding to a 30% variation, in relative terms. Regardless of albedo product used, field data were systematically underestimated by PolDER retrievals. The lowest underestimation corresponded to the use of diurnal course, with an ABias of -5.5 $W.m^{-2}$. A similar bias was observed with the daily mean value. The largest underestimation corresponded to the use of albedo at solar noon (ABias of-12.5 $W.m^{-2}$). As compared to the use of either noon or daily mean value, intermediary underestimations were observed with instantaneous values at 10:00 and 14:00 local solar time, the latter providing very similar ARMSE and ABias.

Table 3

7. Discussion

The intercomparison of the Li - Ross and Roujean retrievals for the diurnal course of hemispherical reflectance was consistent with our knowledge of the considered processes. Curves displayed by Figure 4 were explained by 1/ a larger surface reflection occurring within the visible domain for the bare soil, and 2/ a larger canopy volume scattering occurring within the Near

Infra Red (NIR) domain for vegetated surfaces. The volume scattering increased as the solar zenith angle increased, which induced well pronounced bowl curves for NIR hemispherical reflectance. The differences between model retrievals depended on the surface type, wavelength and solar direction, which may be explained by the different ways the models described the reflection / scattering processes through their kernel formulations.

The intercomparison of the three model retrievals for the diurnal course of hemispherical reflectance mainly showed lower agreements as the solar zenith angle increased (Figure 5). This resulted from 1/ intrinsic capabilities of the reciprocal KD BRDF models for solar extrapolation, especially at large solar zenith angles [*Lucht*, 1998] and 2/ errors in model fitting of PolDER BRDF during the inversion procedure [*Jacob et al.*, 2002b], which drove solar extrapolation performances. We expected in a first time that model retrievals would agree more for the solar positions corresponding to PolDER data acquisition, since they were inverted for these solar positions (see § 3.2). However, the best agreements between model retrievals did not corresponded the PolDER overpass times. This showed that the discrepancies between model retrievals were mainly driven by the different ways the models characterized the BRDF solar dependence.

When intercomparing the model retrievals for the diurnal course of albedo, we observed similar trends to those reported for the diurnal course of NIR hemispherical reflectance. First, the diurnal courses for both variables were bowl curved. Second, the discrepancy between models retrievals were very close: 10% for albedo, and 9% for NIR hemispherical reflectance. Third, the intercomparison scatterplots for both variables were very similar. These results showed the strong link between the two variables, which was explained by two factors. First, the largest hemispherical reflectance values occurred at 865 nm, as shown by Figure 4. Second, the coefficient set to be applied for NTB conversion yielded a large weight to the NIR hemispherical

reflectance (Table 1). These two combined factors induced a larger contribution for NIR hemispherical reflectance to the albedo calculations.

The comparison of the retrieved diurnal courses of albedo against field measurements showed larger differences for larger solar zenith angles (Figure 6). This was explained by three factors. The first one was the performances of the reciprocal KD BRDF models for extrapolating BRDF at large solar zenith angles, also driven by model performances for fitting the observed BRDF. The second factor was the use of models assuming constant surface and meteorological conditions over the diurnal cycle, whereas these conditions could change [*Minnis et al.*, 1997; *Song*, 1998; *Grant et al.*, 2000]. The third factor was assuming a constant diurnal cycle for the ratio of diffuse to direct solar irradiances, when inverting the reciprocal KD BRDF model (§ 4.3). This was different from actual situations, especially for largest solar zenith angles (§ 6.1).

The validation exercises for the several PolDER albedo products we considered indicated the good quality of these products (Table 2). Indeed, Absolute Root Mean Square Error (ARMSE) ranged from 0.0141 to 0.0285, which overlapped the lowest part of the accuracy interval required for further applications (from 0.02 to 0.05, see Introduction). The lowest ARMSE values corresponded to instantaneous values at solar noon and PolDER data acquisition time. The largest ARMSE values for the diurnal course were explained by the inability of the proposed method to retrieve exactly albedo variation over the diurnal cycle, because of the three factors listed in the previous paragraph. It was not surprising to obtain better validation results for the daily mean value of albedo than for the diurnal course. Indeed, the computation of the daily mean value consisted of weighting each instantaneous value with the corresponding solar irradiance (see Equation 5). This yielded lower weights to instantaneous values at large solar zenith angles, and therefore lower contributions from the corresponding largest inaccuracies.

An important result was the 80% correlation coefficient between the retrieval quality for the instantaneous value of albedo at the PolDER data acquisition time and that for the diurnal course of albedo. This underlined the consistency of deriving the diurnal course of albedo by choosing the most adequate coefficient set for the instantaneous value at the PolDER data acquisition time (§ 4.5). More important, it showed the method performances for temporal extrapolation was strongly influenced by those for estimating instantaneous albedo at the data acquisition time. Also, it emphasized the critical points of the method. The first one was the model performances for retrieving the observed BRDF, especially outside of the PolDER angular sampling, since it drove the retrieval quality for the instantaneous value of hemispherical reflectance [*Jacob et al.*, 2002b]. The second critical point was the performance of NTB conversion for spectral extrapolation, to compute the integrated value of albedo [*Jacob et al.*, 2002c].

By inverting reciprocal KD BRDF models over PolDER directional samplings of apparent BRDF, we assumed a constant diurnal course for the ratio of diffuse to direct solar irradiances (§ 4.3). It was not a critical point, since the diffuse solar irradiance decreased as the wavelength increased, and was low for NIR hemispherical reflectance which was the main component for albedo computation (see third paragraph of this section). This was consistent with analysis of the field data displayed on third subplot of Figure 1. Indeed, we constructed a diurnal course of solar irradiance by assuming a constant diurnal course for the ratio of diffuse to direct solar irradiances, and equal to that for PolDER data acquisition time. Its comparison with actual field data showed a relative difference of 5.2%.

Regardless of considered albedo product, the validation results were systematically better with the Li - Ross model. This was consistent with previous studies focusing on the performances of KD BRDF models for providing BRDF - derived products [*Wanner et al.*, 1997;

Privette et al., 1997; *Lucht*, 1998; *Weiss et al.*, 2002b; *Jacob et al.*, 2002b, c; *Schaaf et al.*, 2002; *van Leeuwen and Roujean*, 2002; *Pokrovsky and Roujean*, 2002; *Pokrovsky et al.*, 2003a]. Since Li - Ross systematically provided flatter diurnal courses of albedo, the PolDER calculations for the daily mean value of albedo underestimated field data in a larger extent when using this model rather than MRPV or Roujean.

By assessing the interest of using instantaneous values of albedo in place of the daily mean value, we obtained similar results to those reported in the literature. Using the instantaneous value at solar noon yield significant underestimations (Figure 3 and 8). This was explained by the increase of the instantaneous albedo when solar zenith angle increased (see Figure 6). On the other hand, using instantaneous values at times close to satellite overpasses (10:00 and 14:00 local solar time) did not yield significant biases. This was in agreement with the suggestion of *Henderson-Sellers and Wilson* [1983], who proposed 9:00 local solar time as an optimum time, for using instantaneous values of albedo in place of the daily mean value.

Regardless of PolDER / Li-Ross albedo products used for the derivation of the diurnal course of reflected solar irradiance, field data were systematically underestimated by remote sensing retrievals (Figure 9 and Table 3). The main results are listed below.

- The largest underestimations were observed when using the instantaneous value of albedo at solar noon, since this albedo value was the lowest of the day. The resulting underestimation occurred mainly for intermediary solar zenith angles, since albedo decreased for lower angles and solar irradiance decreased for larger angles.

- The use of the diurnal course of albedo provided the lowest underestimation. This was the best result we could obtain, and corresponded to the accuracy of the method we propose here.

• Underestimations were similar if using the diurnal course or the daily mean value of albedo, since the latter was calculated as the weighted sum of each instantaneous value (see Equation 5). Then, the large scatter around solar noon was explained by the combined effect of 1/ usually larger albedos through the daily mean value, and 2/ a larger solar irradiance at solar noon.

• As compared to the use of either the instantaneous value of albedo at solar noon or the daily mean value of albedo, intermediate underestimations were observed with the instantaneous values at either 10:00 or 14:00 local solar time. Indeed, these albedo values were intermediate between the daily mean value and the instantaneous value at solar noon.

• The similar validation results obtained when using 10:00 and 14:00 albedo values were explained by the low differences between the field data for these albedo values (see Figure 2 and § 6.1). Indeed, analyzing field measurements of albedo showed that, for the Alpilles / ReSeDA experiment, the changes in environmental conditions did not dramatically affect the symmetrical nature of the diurnal course of albedo (§ 6.1).

• Using either the diurnal course of albedo, the daily mean value of albedo, or the instantaneous values of albedo did not affect dramatically the accuracy on the diurnal course of reflected solar irradiance. Indeed, the validation results showed accuracies better than that commonly required, i.e. 20 $W.m^{-2}$ [*van Leeuwen and Roujean*, 2002].

Observing similar product qualities for the reflected solar irradiance regardless of considered albedo product was not in agreement with previous studies. Indeed, the latter reported larger errors if not considering the diurnal course [*Kimes et al.*, 1987; *Grant et al.*, 2000]. The explanation was then the considered environmental conditions, which may have larger consequences than those observed for Alpilles / ReSeDA [*Minnis et al.*, 1997; *Song*, 1998; *Grant et al.*, 2000].

8. Conclusion

This study aimed at proposing a new method for deriving the diurnal course of albedo, by using remote sensing data collected from multiangular sun - synchronous sensors, under clear sky conditions. The method is based on the use of both reciprocal Kernel - Driven (KD) Bi - directional Reflectance Distribution Function (BRDF) models and Narrowband To Broadband (NTB) conversion. Its interest is not requiring local calibration. Its analysis and validation was possible thanks to the richness of the dataset collected during the ReSeDA experiment, which included 20 m spatial resolution airborne PolDER data collected near solar noon, and field measurements of albedo recorded over the diurnal cycle. The investigations reported in the current paper provide useful information for the modeling of BRDF and albedo, and also for the operational use of multiangular sun - synchronous sensors when retrieving land surface albedo.

These investigations underlined the abilities of the reciprocal KD BRDF models to extrapolate the remotely sensed information collected at a given time of the day, for the derivation of land surface albedo over the diurnal cycle. This is an indicator of the model consistencies, and provided new applications, additionally to their operational use for retrieving numerous surface variable products [*Weiss et al.*, 1999; *Weiss and Baret*, 1999; *Weiss et al.*, 2002a; *Liang et al.*, 2002a; *Schaaf et al.*, 2002; *Petitcolin and Vermote*, 2002; *Jacob et al.*, 2004]. Amongst the reciprocal KD BRDF models we selected for conducting this study, better results were systematically obtained with the Li - Ross model. This was consistent with previous studies, and encourages the consideration of this model for related investigations.

A possible improvement of the method we propose would be increasing the modeling degree, by discriminating diffuse and direct components of solar irradiance, when inverting the reciprocal KD BRDF models. This would allow accounting for the diurnal cycle of the ratio of

diffuse to direct solar irradiances. However, it seems to be of second order, since the retrieval quality for the diurnal course of albedo was mainly driven by that for the instantaneous value at the PolDER data acquisition time. Consequently, it is recommended to focus first on better estimating instantaneous retrievals of BRDF, hemispherical reflectance and albedo, when seeking a better accuracy. Nevertheless, the errors we obtained for the different albedo products we considered (instantaneous values at specific times, diurnal course and daily mean value) were included within the range of required accuracies for further applications.

The instantaneous values of albedo at times close to satellite overpasses agreed very well with daily mean values. On the other hand, the qualities of the instantaneous values were better than those of the daily mean value derived from the diurnal course. Then, it is recommended to use instantaneous values at satellite overpasses for the daily mean value, when the latter is needed.

Regardless of considered albedo product used for the derivation of reflected solar irradiance, the quality of the retrievals was better than that required for further applications. This means that instantaneous values, which corresponded to the best accuracies, can be used in place of more complex products such as the diurnal course and the daily mean value. On the other hand, it may be necessary to use the diurnal course of albedo when describing the energetic exchanges with a hourly time step. Indeed, significant differences were observed for middle morning and middle afternoon values. Finally, the daily mean value (respectively the diurnal course), corresponding to the lowest bias (respectively lowest ARMSE), were the most accurate for applications at the daily scale (respectively hourly scale).

These conclusions were not in agreement with others previously reported in the literature. This is probably due to the environmental conditions during the ReSeDA experiment. Indeed, these conditions did not induce significant asymmetries for the diurnal course of albedo, con-

versely to other experiments. Thus, the method proposed in this study might have lower performances for environmental conditions inducing larger asymmetries for the diurnal course of albedo. Then, the question is the occurrence of these asymmetries at the global scale.

Further, it should be interesting to extend the investigations of this study to the retrieval of the other surface variables which drive the diurnal course of net radiation. This may provide new possibilities, when dealing with the strategy of remote sensing data assimilation into SVAT models, such as assimilating net radiation retrievals by considering either instantaneous values at a given time, or diurnal courses.

Acknowledgments. The Alpilles / ReSeDA project was funded by the EEC - DG XII (contract ENV4-CT96-0326-PL952071) and the French *Programme National de Télédétection Spatiale* and *Programme National de Recherches en Hydrologie*. The airborne PolDER sensor was provided by the *Laboratoire d'Optique Atmosphérique*, Lille, France. Financial support was provided by EC in the frame of the WATERMED project (contract ICA3-CT-1999-00015). This study was initiated during a post - doctoral position funded by the ASTER project of NASA's EOS - Terra Program thanks to Tom Schmugge. It was finalized during a visiting period at the U.S. Water Conservation Lab (USDA / ARS, Phoenix, AZ, USA), funded by both NASA under Grant EOS03-0057-0459 (P.I. Andrew French), and the Department of Research, Development, and International Relations of the École Supérieure d'Agriculture de Purpan. Special thanks to Frédéric Baret and Jean-Louis Roujean for constructive discussions, and to the reviewers for increasing the manuscript quality through their comments. We are grateful to the GNU / Octave community for providing a free and powerful numerical computation software.

References

Baret, F., ReSeDA, Assimilation of multisensor and multitemporal remote sensing data to monitor soil and vegetation functioning, *Final Report*, EC research project, 2000.

Baret, F., M. Weiss, M. Leroy, O. Hautecoeur, R. Santer, and A. Bégué, Impact of surface anisotropies on the observation of optical imaging sensors, final report, *ESA contract 11341/95/NL/CN*, ESA, ESTEC, the Netherlands, 1997.

Baret, F., R. Vintila, C. Lazar, R. Rochdi, L. Prévot, C. Lauvernet, J. C. Favard, H. de Boissezon, E. Petcu, G. Petcu, P. Voicu, J. P. Denux, V. Poenaru, C. Simota, O. Marloie, F. Cabot, and P. Henry, *Proceedings of the International Conference "Soils under Global Change - a Challenge for the 21st Century", 3-6 Sept 2002, Constanta (Romania)*, in , 2002.

Barnsley, M., P. Hobson, A. Hyman, W. Lucht, J.-P. Muller, and A. Strahler, Characterizing the spatial variability of broadband albedo in a semi desert environment for MODIS validation, *Remote Sensing of Environment, 74*, 58–68, 2000.

Bastiaanssen, W., and L. Chandrapala, Water balance variability across Sri Lanka for assessing agricultural and environmental water use, *Agricultural Water Management, 58*, 171–192, 2003.

Brasa-Ramos, A., F. De Santa Olalla, V. Caselles, and A. Jochum, Comparison of evapotranspiration estimates by NOAA-AVHRR images and aircraft flux measurements in a semiarid region of Spain, *Journal of Agricultural Engineering Research, 285-294*, 70, 1998.

Brest, C., and S. Goward, Deriving surface albedo measurements from narrow band satellite data, *International Journal of Remote Sensing, 8*, 351–367, 1987.

Chopping, M., Testing a LiSK BRDF Model with in Situ Bidirectional Reflectance Factor Measurements over Semiarid Grasslands, *Remote Sensing of Environment, 74*, 287–312, 2000.

Cihlar, J., R. Barry, O. Gil, K.-I. Kuma, J. Landwerh, D. Norse, S. Running, R. Scholes, A. Solomon, and S. Whao, GCOS/GTOS plan for terrestrial climate-related observations, Version 2.0, *GCOS-32 WMO/TD-No 796, UNEP/DEIA/TR.97.7*, GCOS Joint Planning Office, Geneva, Switzerland, 1997.

Courault, D., P. Lacarrere, P. Clastre, P. Lecharpentier, F. Jacob, O. Marloie, L. Prévot, and A. Olioso, Estimation of surface fluxes in a small agricultural area using the three-dimensional atmospheric model Meso-NH and remote sensing data, *Canadian Journal of Remote Sensing*, *29*, 741–754, 2003.

Dedieu, G., P. Deschamps, and Y. Kerr, Satellite estimation of solar irradiance at the surface of the Earth and of surface albedo using a physical model applied to Meteosat data, *Journal of Climate and Applied Meteorology*, *26*, 79–87, 1987.

Dickinson, R., Land surface processes and climate-surface albedos and energy balance, *Advances in Geophysics*, *25*, 305–353, 1983.

Dickinson, R., B. Pinty, and M. Verstraete, Relating surface albedos in GCM to remotely sensed data, *Agricultural and Forest Meteorology*, *52*, 109–131, 1990.

Engelsen, O., B. Pinty, M. Verstraete, and J. Martonchik, Parametric bidirectional reflectance factor models : evaluation, improvements and applications, *Report EUR16426EN*, European Commission, Joint Researches Center, Space Application Institute, ISPRA, Italy, 1996.

François, C., C. Ottlé, A. Olioso, L. Prévot, N. Bruguier, and Y. Ducros, Conversion of 400 - 1100 nm vegetation albedo measurements into total shortwave broadband albedo using a canopy radiative transfer model, *Agronomie: Agriculture and Environment*, *22*, 611–618, 2002.

Grant, I., A. Prata, and R. Ceche, The impact of the diurnal variation of albedo on the remote sensing of the daily mean albedo of grassland, *Journal of Applied Meteorology*, *39*, 231–244, 2000.

Henderson-Sellers, A., and M. Wilson, Surface albedo data for climatic modeling, *Reviews on Geophysics*, *23*, 1743–1778, 1983.

Jackson, R., Evaluating evapotranspiration at local and regional scale, *Proceedings of the IEEE*, *73*, 1086–1096, 1985.

Jacob, F., A. Olioso, X. Gu, Z. Su, and B. Seguin, Mapping surface fluxes using visible, near infrared, thermal infrared remote sensing data with a spatialized surface energy balance model, *Agronomie: Agriculture and Environment*, *22*, 669–680, 2002a.

Jacob, F., A. Olioso, M. Weiss, F. Baret, and O. Hautecoeur, Mapping short-wave albedo of agricultural surfaces using airborne PolDER data, *Remote Sensing of Environment*, *80*, 36–46, 2002b.

Jacob, F., M. Weiss, A. Olioso, and A. French, Assessing the narrowband to broadband conversion to estimate visible, near infrared and shortwave apparent albedo from airborne PolDER data, *Agronomie: Agriculture and Environment*, *22*, 537–546, 2002c.

Jacob, F., F. Petitcolin, T. Schmugge, E. Vermote, K. Ogawa, and A. French, Comparison of land surface emissivity and radiometric temperature from MODIS and ASTER sensors, *Remote Sensing of Environment*, *83*, 1–18, 2004.

Kimes, D., and P. Sellers, Inferring hemispherical reflectance of the Earth's surface for global energy budgets from remotely sensed nadir or directional radiance values, *Remote Sensing of Environment*, *18*, 205–223, 1985.

Kimes, D., P. Sellers, and W. Newcomb, Hemispherical reflectance variations of vegetation canopies and implications for global and regional energy budget studies, *Journal of Climate and Applied Meteorology*, *26*, 959–972, 1987.

Kimes, D., Y. Knyazikhin, J. Privette, A. Abuelgasim, and F. Gao, Inversion methods for Physically-Based Models, *Remote Sensing Reviews*, *18*, 381–439, 2000.

Kustas, W., and K. Humes, Spatially distributed sensible heat flux over a semiarid watershed. Part II : use of a variable resistance approach with radiometric surface temperatures, *Journal of Applied Meteorology*, *36*, 293–301, 1997.

Kustas, W., and J. Norman, Evaluation of soil and vegetation heat flux predictions using a simple two-source model with radiometric temperatures for partial canopy cover, *Agricultural and Forest Meteorology*, *94*, 13–29, 1999.

Leroy, M., and O. Hautecoeur, Directional parameters, hemispherical reflectances and angle-corrected NDVIs derived at global scale by the spaceborne PolDER, in *Proceedings of Alps 1999 conference, Méribel, France, January 18-22, 'Land surface' session*, edited by CNES, pp. 1–4, 1999.

Liang, S., Narrowband to broadband conversions of land surface albedo I Algorithms, *Remote Sensing of Environment*, *76*, 213–238, 2000.

Liang, S., and A. Strahler, An analytic BRDF model of canopy radiative transfer and its inversion, *IEEE Transaction on Geoscience and Remote Sensing*, *31*, 1081–1092, 1993.

Liang, S., A. Strahler, and C. Walthall, Retrieval of land surface albedo from satellite observations: A simulation study, *Journal of Applied Meteorology*, *38*, 712–725, 1999.

Liang, S., H. Fang, M. Chen, C. Shuey, C. Walthall, C. Daughtry, J. Morisette, C. Schaaf, and A. Strahler, Validating MODIS land surface reflectance and albedo products: methods and

preliminary results, *Remote Sensing of Environment*, *83*, 83, 2002a.

Liang, S., C. Shuey, A. Russ, H. Fang, M. Chen, C. Walthall, C. Daughtry, and R. Hunt, Narrowband to broadband conversions of land surface albedo II Validation, *Remote Sensing of Environment*, *84*, 25–41, 2002b.

Lucht, W., Expected retrieval accuracies of bidirectional reflectance and albedo from EOS-MODIS and MISR angular sampling, *Journal of Geophysical Research*, *103*, 8763–8778, 1998.

Lucht, W., and J. Roujean, Considerations in the parametric modeling of BRDF and albedo from multiangular satellite sensor observations, *Remote Sensing Reviews*, *18*, 343–379, 2000.

Lucht, W., C. Schaaf, and A. Strahler, An algorithm for the retrieval of albedo from space using semi-empirical BRDF models, *IEEE Transactions on Geoscience and Remote Sensing*, *38*, 977–997, 2000.

Minnis, P., S. Mayor, S. Jr., W.L., and D. Young, Assymetry in the diurnal variation of surface albedo, *IEEE Transactions on Geoscience and Remote Sensing*, *35*, 879–891, 1997.

Moran, M., W. Kustas, A. Vidal, D. Stannard, J. Blanford, and W. Nichols, Use of ground-based remotely sensed data for surface energy balance evaluation of a semiarid rangeland, *Water Resources Research*, *30*, 1339–1349, 1994.

Myhre, G., and A. Myhre, Uncertainties in radiative forcing due to surface albedo changes caused by land-use changes, *Journal of Climate*, *16*, 1511–1524, 2003.

Nilson, T., and A. Kuusk, A reflectance model for the homogeneous plant canopy and its inversion, *Remote Sensing of Environment*, *27*, 157–167, 1989.

Noilhan, J., and P. Lacarrere, GCM grid-scale evaporation from mesoscale modeling, *Journal of Climate*, *8*, 206–223, 1995.

Olioso, A., L. Prévot, F. Baret, A. Chanzy, I. Braud, H. Autret, F. Baudin, P. Bessemoulin, O. Bethenod, D. Blamont, B. Blavoux, J. Bonnefond, S. Boubkraoui, B. Bouman, N. Bruguier, J. Calvet, V. Caselles, H. Chauki, J. Clevers, C. Coll, A. Company, D. Courault, G. Dedieu, P. Degenne, R. Delécolle, H. Denis, J. Desprats, Y. Ducros, D. Dyer, J. Fies, A. Fischer, C. Francois, J. Gaudu, E. Gonzalez, R. Gouget, X. Gu, M. Guérif, J. Hanocq, J. Hautecoeur, R. Haverkamp, S. Hobbs, F. Jacob, R. Jeansoulin, R. Jongschaap, Y. Kerr, C. King, P. Laborie, J. Lagouarde, A. Laques, D. Larcena, G. Laurent, J. Laurent, M. Leroy, J. McAneney, G. Macelloni, S. Moulin, J. Noilhan, C. Ottlé, S. Paloscia, P. Pampaloni, T. Podvin, F. Quaracino, J. Roujean, C. Rozier, R. Ruisi, C. Susini, O. Taconet, N. Tallet, J. Thony, Y. Travi, H. Van Leewen, M. Vauclin, D. Vidal-Madjar, O. Vonder, M. Weiss, and J. Wigneron, Spatial aspects in the Alpilles-ReSeDA project, in *Scaling and modeling in forestry: application in remote sensing and GIS, Ed. D.Marceau, Université de Montréal, Québec*, edited by D. Marceau, pp. 92–102, 1998.

Olioso, A., I. Braud, A. Chanzy, J. Demarty, Y. Ducros, J. Gaudu, E. Gonzales-Soza, L. Lewan, O. Marloie, C. Ottlé, L. Prévot, J.-L. Thony, H. Autret, I. Bethenod, J. Bonnefond, N. Brugier, J.-P. Buis, J.-C. Calvet, V. Caselles, H. Chauki, C. Coll, C. François, R. Goujet, R. Jongschaap, Y. Kerr, C. King, J.-P. Lagouarde, J.-P. Laurent, P. Lecharpentier, J. McAnneney, S. Moulin, E. Rubio, M. Weiss, and J.-P. Wigneron, Monitoring energy and mass transfers during the Alpilles-ReSeDA experiment, *Agronomie: Agriculture and Environment*, *22*, 597–610, 2002.

Ottlé, C., and D. Vidal-Madjar, Assimilation of soil moisture inferred from infrared remote sensing in a hydrological model over the HAPEX-MOBILHY region, *Journal of Hydrology*, *158*, 241–264, 1994.

Petitcolin, F., and E. Vermote, Land surface reflectance, emissivity and temperature from MODIS middle and thermal infrared data, *Remote Sensing of Environnement*, *83*, 112–134, 2002.

Pinty, B., and D. Tanré, The relationship between incident and double-way transmittances: an application for the estimate of surface albedo from satellite over the African Sahel, *Journal of Climate and Applied Meteorology*, *41*, 893–896, 1987.

Pinty, B., and M. Verstraete, On the design and validation of surface bidirectional reflectance and albedo model, *Remote Sensing of Environment*, *41*, 155–167, 1992.

Pinty, B., F. Roveda, M. Verstraete, N. Gobron, Y. Govaerts, J. Martonchik, D. Diner, and R. Kahn, Surface albedo retrieval from Meteosat 1. Theory, *Journal of Geophysical Research*, *105*, 18,099–18,112, 2000a.

Pinty, B., F. Roveda, M. Verstraete, N. Gobron, Y. Govaerts, J. Martonchik, D. Diner, and R. Kahn, Surface albedo retrieval from Meteosat 2. Applications, *Journal of Geophysical Research*, *105*, 18,113–18,134, 2000b.

Pokrovsky, I., and J. Roujean, Land surface albedo retrieval via kernel-based BRDF modeling: I. Statistical inversion method and model comparison, *Remote Sensing of Environment*, *84*, 100–119, 2002.

Pokrovsky, I., O. Pokrovsky, and J. Roujean, Development of an operational procedure to estimate surface albedo from the SEVIRI/MSG observing system by using POLDER BRDF measurements I. Data quality control and accumulation of information corresponding to the IGBP land cover classes, *Remote Sensing of Environment*, *87*, 198–214, 2003a.

Pokrovsky, I., O. Pokrovsky, and J. Roujean, Development of an operational procedure to estimate surface albedo from the SEVIRI/MSG observing system by using POLDER BRDF

measurements II. Comparison of several inversion techniques and uncertainty in albedo estimates, *Remote Sensing of Environment*, *87*, 215–242, 2003b.

Pragnère, A., F. Baret, M. Weiss, R. Myneni, Y. Knyazikhin, and L. Wang, Comparison of three radiative transfer model inversion techniques to estimate canopy biophysical variables from remote sensing data, in *Proceedings of IGARSS 1999, 28 June - 2 July 1999, Hamburg*, vol. 2, edited by T. Stein, pp. 1093–1095, 1999.

Privette, J., T. Eck, and D. Deering, Estimating spectral albedo and nadir reflectance through inversion of simple BRDF models with AVHRR/MODIS-like data, *Journal of Geophysical Research*, *102*, 29,529–29,542, 1997.

Prévot, L., F. Baret, A. Chanzy, A. Olioso, J. Wigneron, H. Autret, F. Baudin, P. Bessemoulin, O. Bethenod, D. Blamont, B. Blavoux, J. Bonnefond, S. Boubkraoui, B. Bouman, I. Braud, N. Bruguier, J. Calvet, V. Caselles, H. Chauki, J. Clevers, C. Coll, A. Company, D. Courault, G. Dedieu, P. Degenne, R. Delécolle, H. Denis, J. Desprats, Y. Ducros, D. Dyer, J. Fies, A. Fischer, C. Francois, J. Gaudu, E. Gonzalez, R. Gouget, X. Gu, M. Guérif, J. Hanocq, J. Hautecoeur, R. Haverkamp, S. Hobbs, F. Jacob, R. Jeansoulin, R. Jongschaap, Y. Kerr, C. King, P. Laborie, J. Lagouarde, A. Laques, D. Larcena, G. Laurent, J. Laurent, M. Leroy, J. McAneney, G. Macelloni, S. Moulin, J. Noilhan, C. Ottlé, S. Paloscia, P. Pampaloni, T. Podvin, F. Quaracino, J. Roujean, C. Rozier, R. Ruisi, C. Susini, O. Taconet, N. Tallet, J. Thony, Y. Travi, H. Van Leewen, M. Vauclin, D. Vidal-Madjar, O. Vonder, and M. Weiss, Assimilation of multi-sensor and multi-temporal remote sensing data to monitor vegetation and soil: the Alpilles ReSeDA project, in *IGARSS'98 International Geoscience and Remote Sensing Symposium, IEEE, Institute of Electrical and Electronics Engineers, Piscataway (USA), Sensing and managing the environment*, vol. 5, edited by L. Tsang, pp. 2399–2401, 1998.

Rahman, H., and G. Dedieu, SMAC : a Simplified Method for the Atmospheric Correction of satellite measurements in the solar spectrum, *International Journal of Remote Sensing*, *16*, 123–143, 1994.

Roujean, J., M. Leroy, and P. Deschamps, A bidirectional reflectance model of the Earth's surface for the correction of remote sensing data, *Journal of Geophysical Research*, *97*, 20,455–20,468, 1992.

Roujean, J., D. Tanre, F.-M. Bréon, and J. Deuzé, Retrieval of land surface parameters from airborne PolDER bidirectional reflectance distribution function during HAPEX-Sahel, *Journal of Geophysical Research*, *102*, 11,210–11,218, 1997.

Russel, M., M. Nunez, M. Chladil, J. Valiente, and E. Lopez-Baeza, Conversion of nadir, narrowband reflectance in red and near infrared to hemispherical surface albedo, *Remote Sensing of Environment*, *61*, 16–23, 1997.

Schaaf, C., F. Gao, A. Strahler, W. Lucht, X. Li, T. Tsang, N. Strugnell, X. Zhang, Y. Jin, J.-P. Muller, P. Lewis, M. Barnsley, P. Hobson, M. Disney, G. Roberts, M. Dunderdale, C. Doll, R. D'Entremont, B. Hu, S. Liang, J. Privette, and D. Roy, First operational BRDF, albedo nadir reflectance products from MODIS, *Remote Sensing of Environment*, *83*, 135–148, 2002.

Seguin, B., and B. Itier, Using midday surface temperature to estimate daily evaporation from satellite data, *International Journal of Remote Sensing*, *4*, 371–383, 1983.

Sellers, P., B. Meeson, F. Hall, G. Asrar, R. Murphy, R. Schiffer, F. Bretherton, R. Dickinson, R. Ellingson, C. Field, K. Huemmrich, C. Justice, J. Melack, N. Roulet, D. Schimel, and P. Try, Remote sensing of the land surface for the global change: models - algorithms - experiments, *Remote Sensing of Environment*, *51*, 3–26, 1995.

Soer, G., The TERGRA model, a mathematical model for the simulation of the daily behavior of crop surface temperature and actual evapotranspiration, *Publ. 46*, NIWARS, Delft, The Netherlands, 1977.

Song, J., Diurnal assymetry in surface albedo, *Agricultural and Forest Meteorology*, *92*, 181–189, 1998.

Song, J., and W. Gao, An improved method to derive surface albedo from narrow-band AVHRR satellite data: narrow-band to broadband conversion, *Journal of Applied Meteorology*, *38*, 239–249, 1999.

Tian, Y., R. Dickinson, L. Zhou, R. Myneni, M. Friedl, C. Schaaf, M. Caroll, and F. Gao, Land boundary conditions from MODIS data and consequences for the albedo of a climate, *Geophysical Research Letters*, *31*, 5pp, 2004.

Toll, D., D. Shirey, and D. Kimes, NOAA AVHRR lans surface albedo algorithm development, *International Journal of Remote Sensing*, *18*, 3761–3796, 1997.

van Leeuwen, W., and J.-L. Roujean, Land surface albedo from the synergistic use of polar (EPS) and geo-stationary (MSG) observing systems. An assessment of physical uncertainties, *Remote Sensing of Environment*, *81*, 273–289, 2002.

Walthall, C., J. Norman, G. Welles, G. Campbell, and G. Blad, Simple equation to approximate the bidirectional reflectance from vegetative canopies and bare soil surfaces, *Applied Optics*, *24*, 383–387, 1985.

Wanner, W., X. Li, and A. Strahler, On the derivation of kernels for kernel-driven models of bidirectional reflectance, *Journal of Geophysical Research*, *100*, 21,077–21,089, 1995.

Wanner, W., A. Strahler, B. Hu, P. Lewis, J.-P. Muller, X. Li, C. Barker Schaaf, and M. Barnsley, Global retrieval of bidirectional reflectance and albedo over land from EOS MODIS and

MISR data: theory and algorithm, *Journal of Geophysical Research, 102*, 17,143–17,161, 1997.

Wassenaar, T., A. Olioso, C. Hasager, F. Jacob, and A. Chehbouni, Estimation of evapotranspiration over heterogeneous pixels, in *Proceedings of the First International Symposium on Recent Advances in Quantitative Remote Sensing, September 2002, Valencia, Spain*, edited by J. Sobrino, pp. 458–465, 2002.

Weiss, M., and F. Baret, Evaluation of Canopy Biophysical Variable Retrival Performances from the Accumulation of Large Swath Satellite Data, *Remote Sensing of Environment, 70*, 293–306, 1999.

Weiss, M., F. Baret, M. Leroy, A. Bégué, O. Hautecoeur, and R. Santer, Hemispherical reflectance and albedo estimate from the accumulation of across-track sun-synchronous satellite data, *Journal of Geophysical Research*, *104*, 22,221–22,232, 1999.

Weiss, M., F. Baret, M. Leroy, O. Hautecoeur, C. Bacour, L. Prévot, and N. Bruguier, Evaluation of Neural Network techniques to estimate canopy biophysical variables from remote sensing data, *Agronomie: Agriculture and Environment*, *22*, 547–553, 2002a.

Weiss, M., F. Jacob, F. Baret, A. Pragnère, C. Bruchou, M. Leroy, O. Hautecoeur, L. Prévot, and N. Bruguier, Evaluation of kernel-driven BRDF models for the normalization of Alpilles/ReSeDA PolDER data, *Agronomie: Agriculture and Environment*, *22*, 531–536, 2002b.

Zhao, W., M. Tamura, and H. Takahashi, Atmospheric and spectral corrections for estimating surface albedo from satellite data using 6S code, *Remote Sensing of Environment*, *76*, 202–212, 2000.

Author	Sensor	Wavebands & Coefficient values				Offset
Liang et al. [1999]	*MISR*	*426-467*	*544-571*	*662-682*	*847-886*	
		0.1587	**-0.2463**	**0.5442**	**0.3748**	**0.0149**

Table 1. Set of coefficients used to compute surface albedo as a linear combination of the hemispherical reflectance within the four PolDER channels (NTB conversion). The coefficients were calibrated considering the MISR filter response functions [*Liang et al.*, 1999].

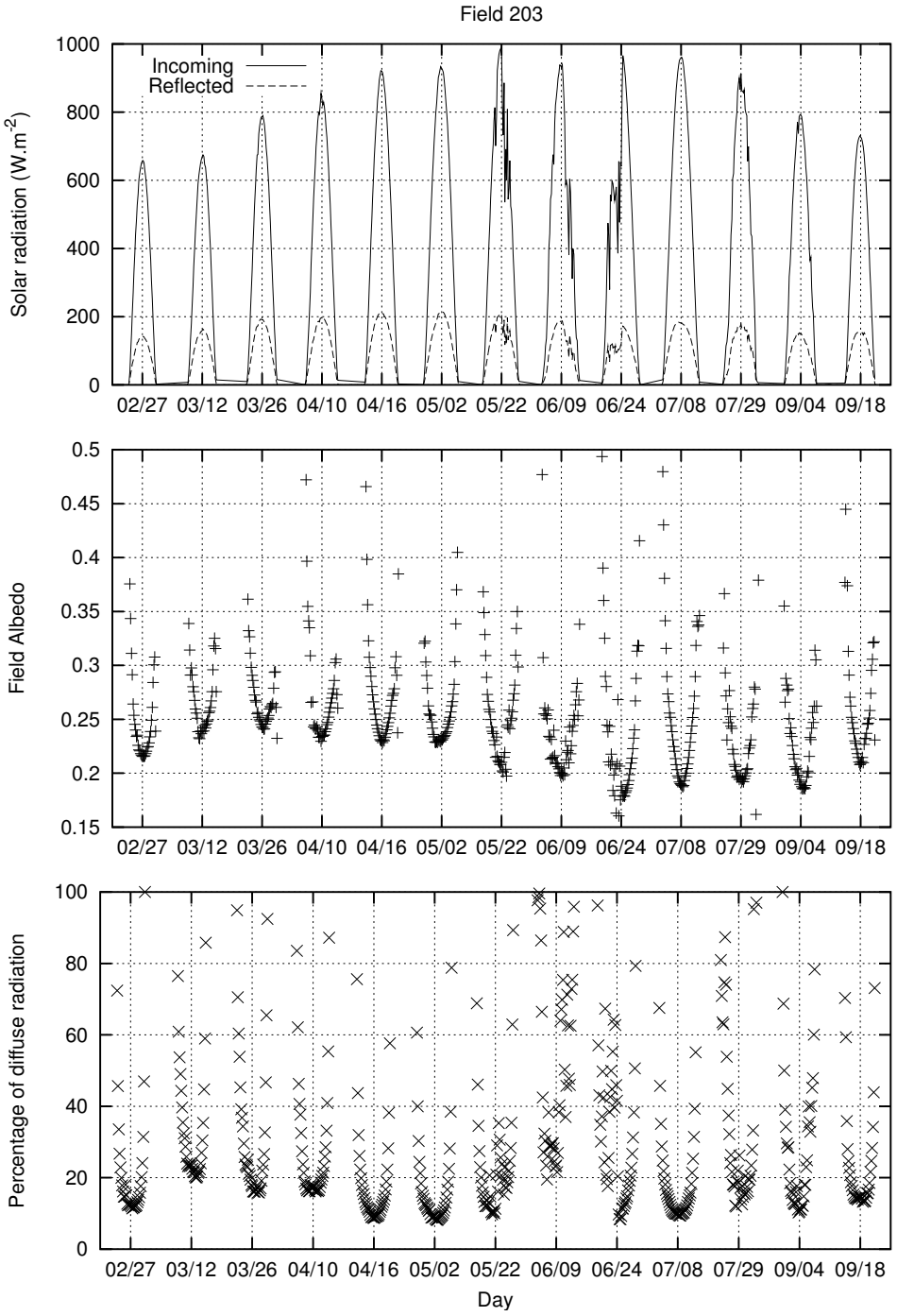

Figure 1. First subplot: diurnal courses of incoming and reflected solar radiation over field 203 (alfalfa). Second subplot: diurnal course of albedo calculated as the ratio of reflected to incoming solar radiation displayed on the first subplot. Third subplot: magnitude of the diffuse solar irradiance, expressed as the ratio of diffuse to total solar irradiances. For these three subplots, the considered days correspond to PolDER data acquisition.

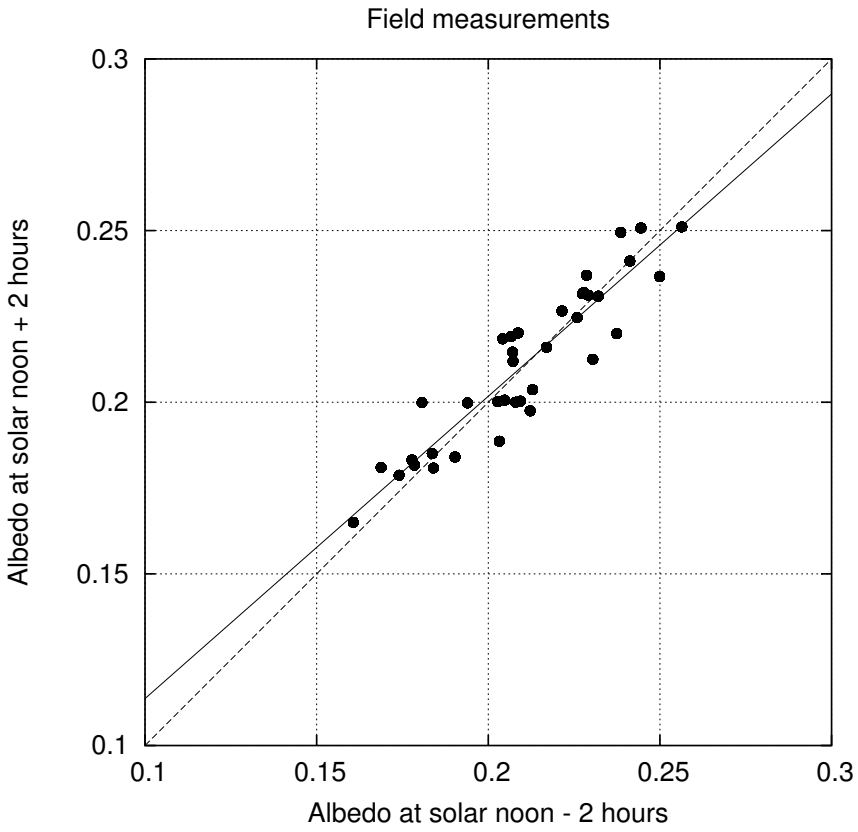

Figure 2. Comparison between field measurements of albedo at local solar noon -2 hours and local solar noon + 2 hours. The dashed line is the 1:1 line. The continuous line corresponds to the regression obtained if expressing albedo at 14:00 local solar time as a linear function of albedo at 10:00 local solar time.

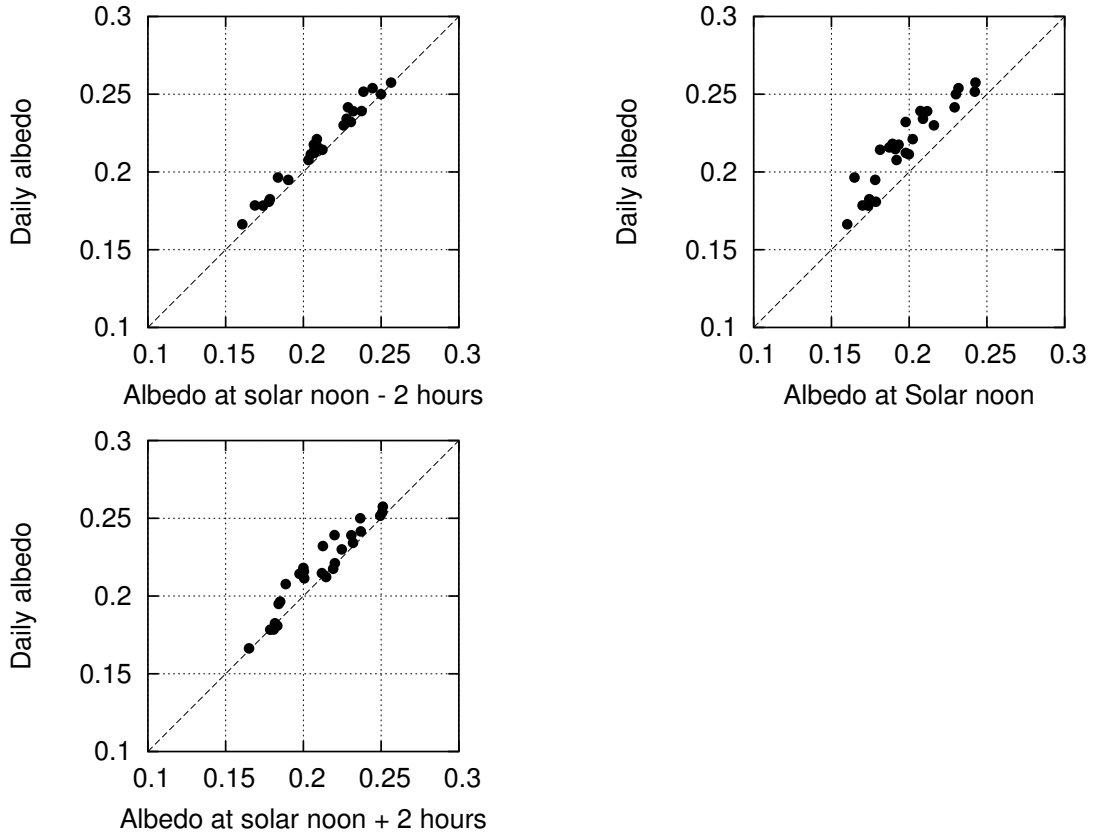

Figure 3. Comparison, against the daily mean values of albedo, of instantaneous albedo values at solar noon and times close to satellite overpasses. Results obtained using field data.

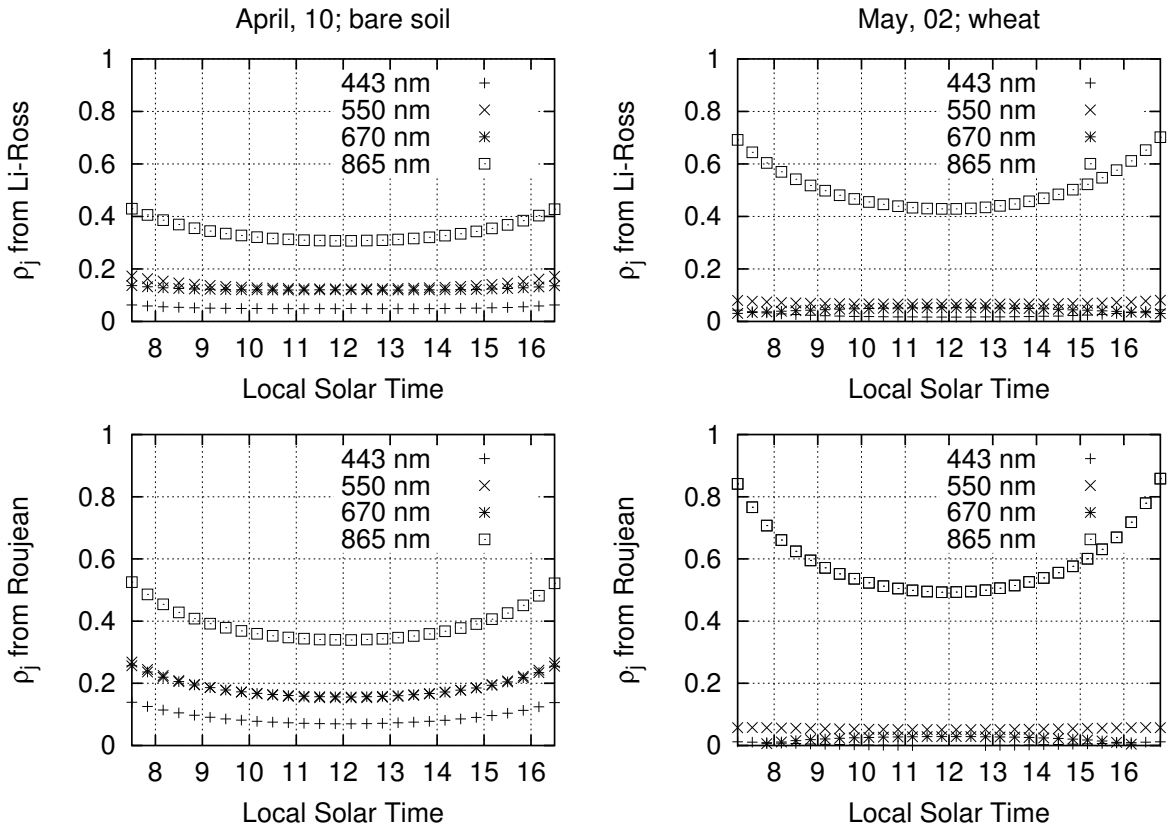

Figure 4. Illustration of retrieved diurnal courses of hemispherical reflectance within the four PolDER channels. We considered two surfaces: a bare soil (left) and a wheat crop with a 1.12 LAI value (right), and two reciprocal KD BRDF models: Li - Ross (top) and Roujean (bottom).

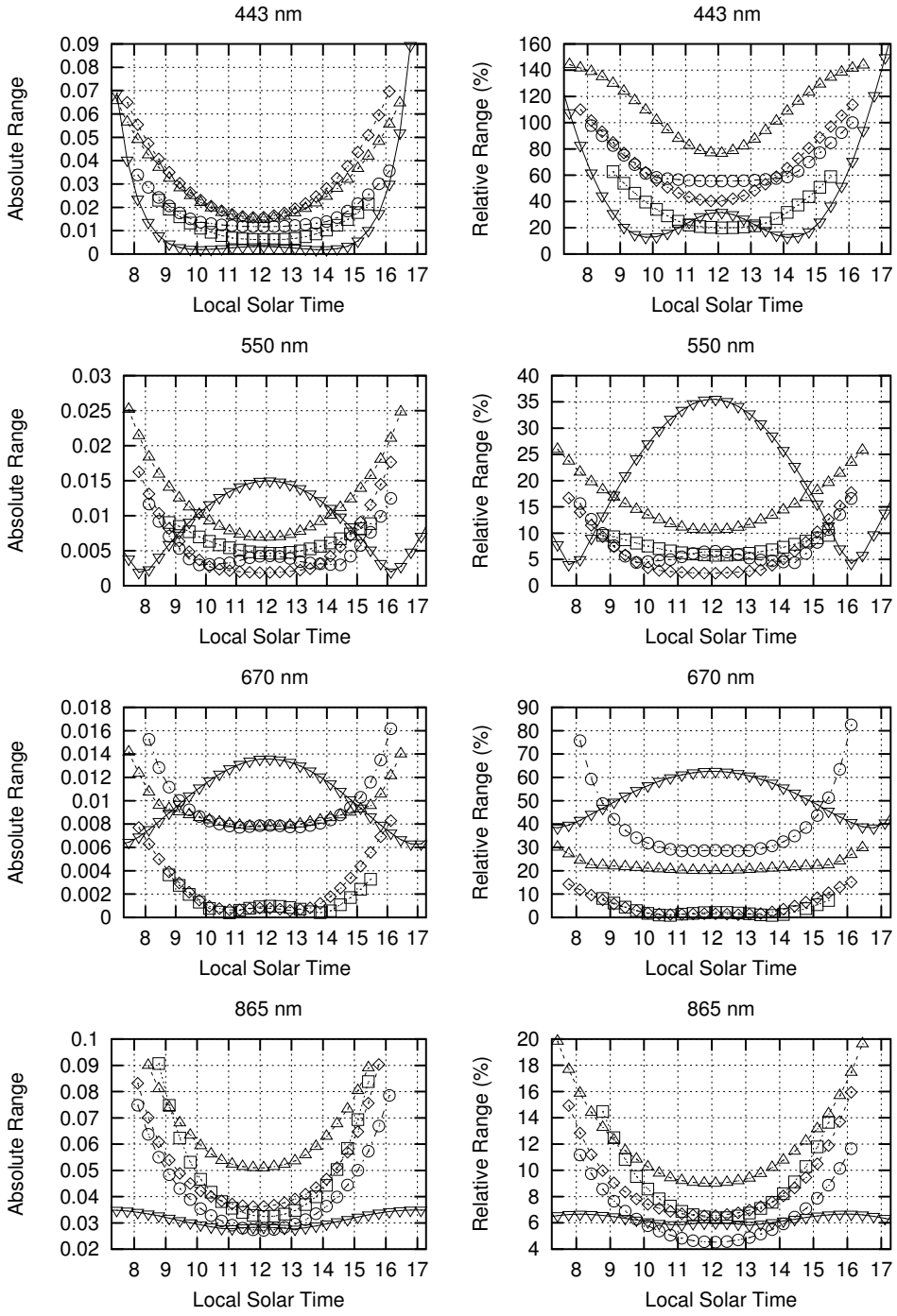

Figure 5. Variation, versus the local solar time, of Absolute (left subplots) and Relative (right subplots) discrepancies between model retrievals of hemispherical reflectance. We considered the four PolDER channels (top to bottom subplots), and the alfalfa crop (field 203). For a better subplot readability, we considered a 2 day step. Each line style corresponds to a given day. Minimum solar zenith angle corresponds to 12:00 local solar time.

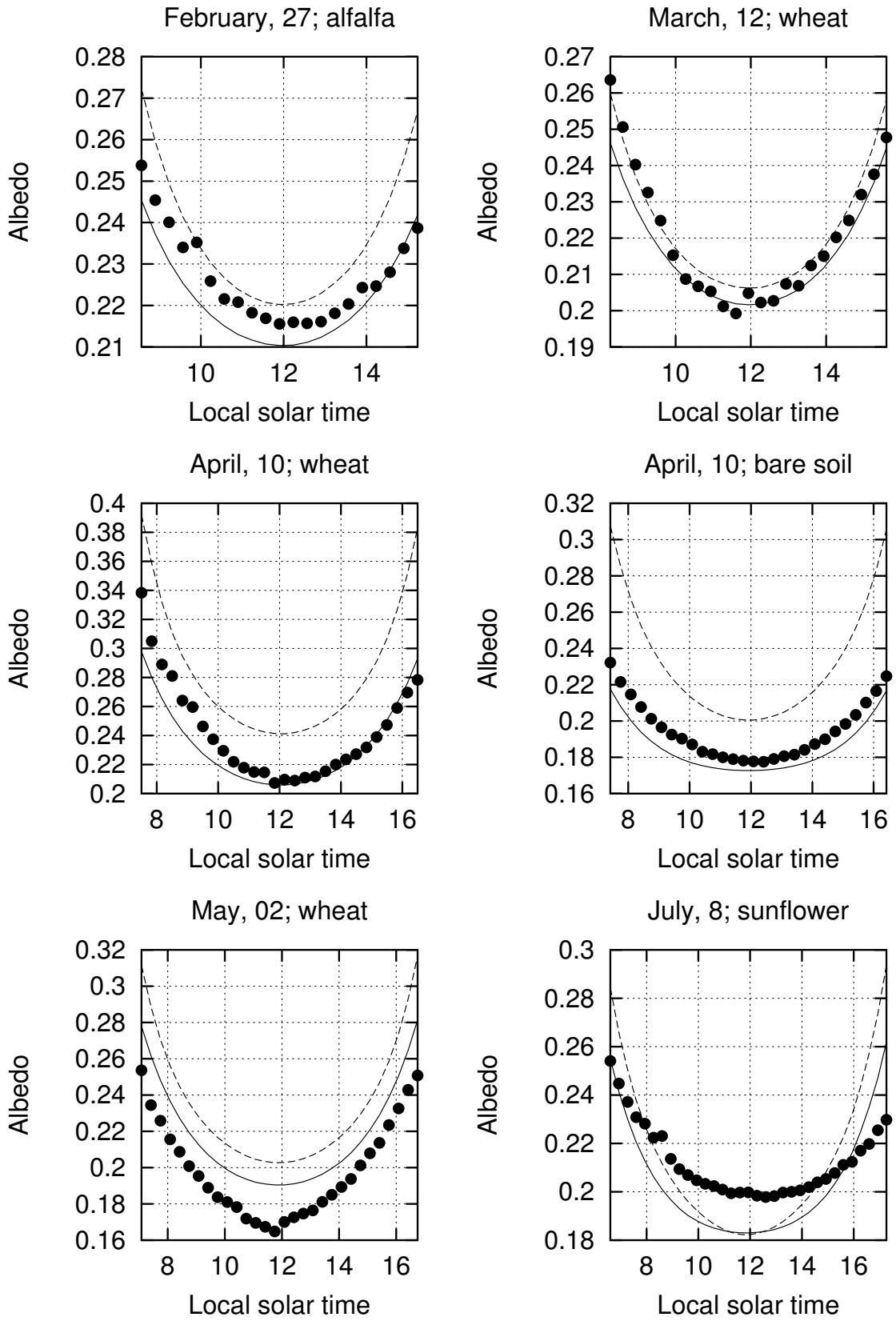

Figure 6. Comparison against field measurements (•) of the diurnal course of albedo retrieved from the Li - Ross (—) and Roujean (- -) reciprocal KD BRDF models.

	Instantaneous value		Diurnal course		Solar noon value		Daily mean value	
Model	ARMSE	ABias	ARMSE	ABias	ARMSE	ABias	ARMSE	ABias
Li - Ross	0.0152	-0.0054	0.0259	-0.0140	0.0141	-0.0029	0.0168	-0.0078
MRPV	0.0179	0.0059	0.0268	0.0029	0.0180	0.0094	0.0258	0.0092
Roujean	0.0190	0.0043	0.0285	-0.0027	0.0201	0.0056	0.0223	0.0070

Table 2. ARMSE and ABias between PolDER albedo retrievals and *in - situ* measurements. From left to right: the instantaneous value at the PolDER data acquisition time, the diurnal course, the instantaneous value at solar noon, and the daily mean value. ARMSE (Absolute Root Mean Square Error) is the mean quadratic difference between predictions and observations for a given variable. RRMSE (Relative Root Mean Square Error) is the ratio of ARMSE to the mean value of the observations. ABias is the mean difference between predictions and observations for a given variable. RBias is the ratio of ABias to the mean value of the observations.

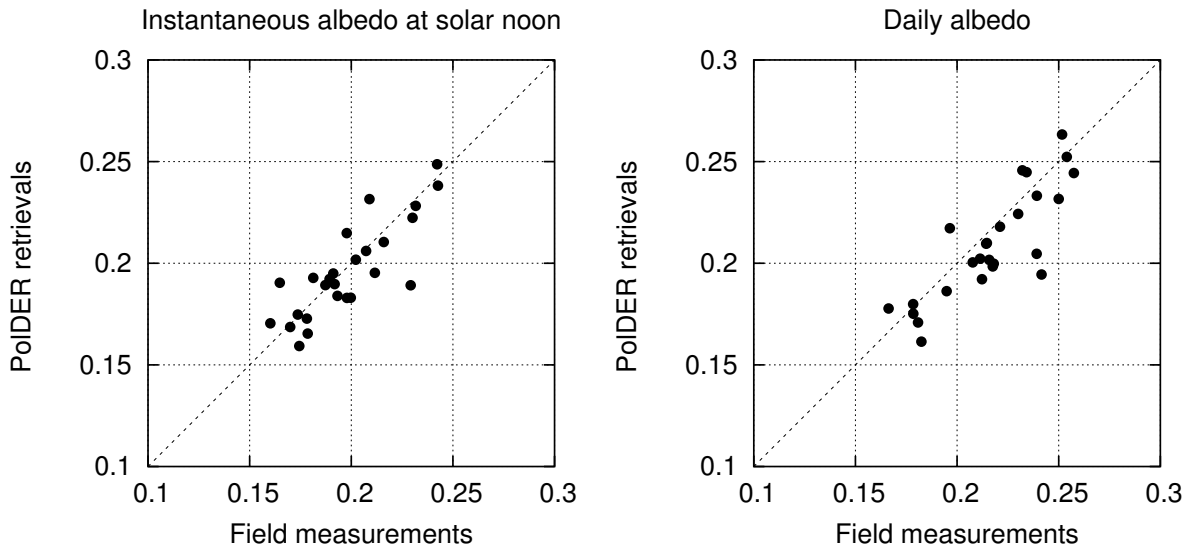

Figure 7. Comparison, against field measurements, of albedo products retrieved from the PolDER data using the Li - Ross model: the instantaneous value at local solar noon (left) and the daily mean value (right).

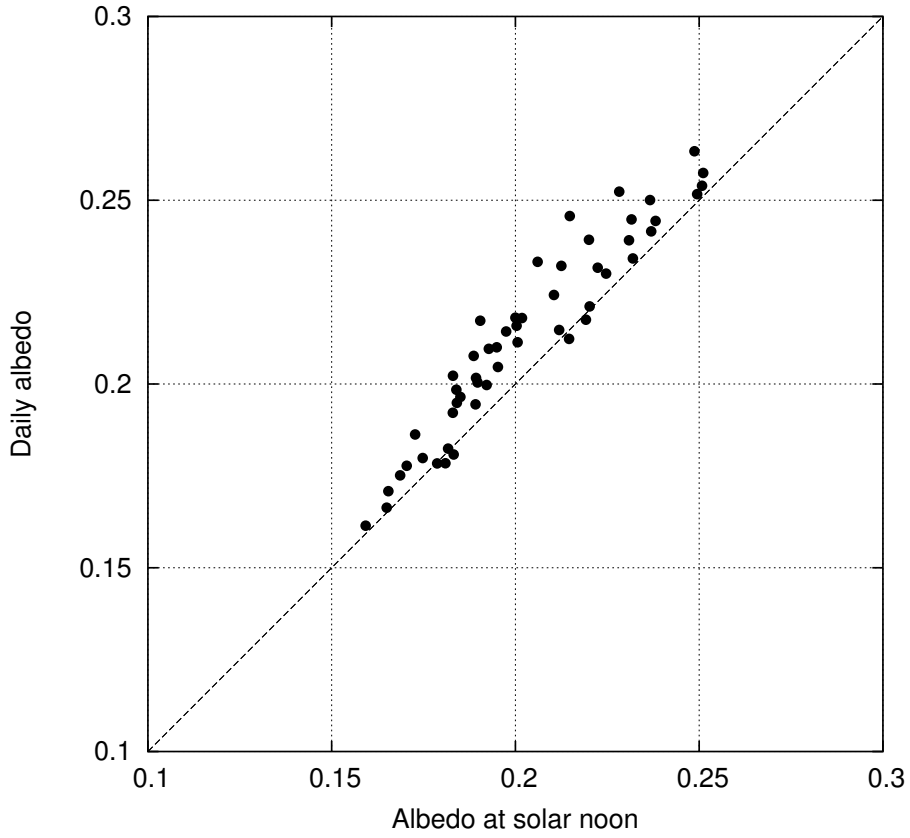

Figure 8. Comparison, against the daily mean values of albedo, of instantaneous albedo values at solar noon. Results obtained using the PolDER / Li - Ross retrievals.

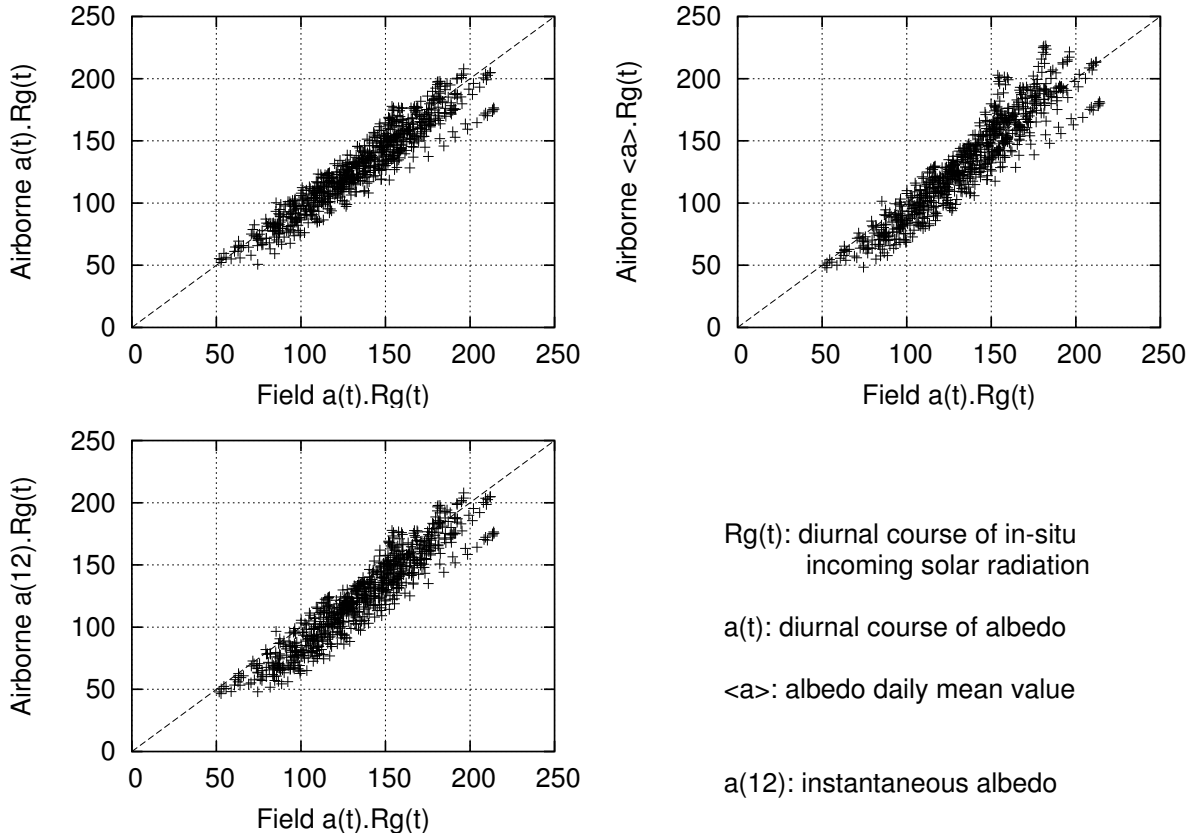

Figure 9. Comparison, against field measurements, of the diurnal course of reflected solar irradiance retrieved from PolDER / Li - Ross by considering 1/ the diurnal course of albedo, 2/ the daily mean value, and 3/ the instantaneous value at solar noon.

Albedo	ARMSE ($W.m^{-2}$)	ABias ($W.m^{-2}$)
Diurnal course	11.47	-5.56
Daily mean Value	14.81	-5.50
Instantaneous value @ 10:00	15.72	-8.53
Instantaneous value @ 12:00	16.78	-12.48
Instantaneous value @ 14:00	15.56	-7.67

Table 3. ARMSE and ABias obtained when validating, against field measurements, the diurnal course of reflected solar irradiance retrieved from PolDER / Li - Ross by considering 1/ the diurnal course of albedo, 2/ the daily mean value, and 3/ the instantaneous values at 10:00, 12:00 and 14:00 local solar time. ARMSE (Absolute Root Mean Square Error) is the mean quadratic difference between predictions and observations for a given variable. RRMSE (Relative Root Mean Square Error) is the ratio of ARMSE to the mean value of the observations. Bias is the mean difference between predictions and observations for a given variable. RBias is the ratio of ABias to the mean value of the observations.